MIXING ANALYSIS IN A STIRRED TANK USING COMPUTATIONAL FLUID DYNAMICS

A THESIS SUBMITTED TO THE DEPARTMENT OF

NUCLEAR ENGINEERING

COLLEGE OF BASIC AND APPLIED SCIENCES

UNIVERSITY OF GHANA

BY

(MATILDA DOTSE, 10507328)

BSC (CAPE COAST), 2012

IN PARTIAL FULFILMENT OF THE REQUIREMENTS FOR THE DEGREE OF

MASTER OF PHILOSOPHY

IN

NUCLEAR TECHNOLOGY APPLICATIONS IN PETROLEUM AND MINING INDUSTRIES

JULY 2016

DECLARATION

This thesis is the result of research work done on "**Mixing Analysis in a Stirred Tank Using Computational Fluid Dynamics"** by Matilda Dotse of the Department of Nuclear Engineering, Graduate School of Nuclear and Allied Sciences, University of Ghana, under the supervision of Dr. C.P.K. Dagadu and Dr Stephen Yamoah.

All information has been acknowledged by means of references.

…… Date: ……

Matilda Dotse

(Student)

…….. Date: ……

Dr. C.P.K. Dagadu

(Supervisor)

..…….. Date: …….....

Dr. Stephen Yamoah

(Supervisor)

DEDICATION

This research work is dedicated to my parents especially my mother, Madam Rita Hortunu, my brother, Benedictus Sitsofe Dotse, and my sister, Ernestine Dotse for their love, prayers and support.

ACKNOWLEDGEMENTS

I am grateful to the Almighty God for His grace and favour towards me throughout this work. I genuinely thank my supervisors, Dr Stephen Yamoah and Dr C.P.K. Dagadu, for the time they devoted in guiding me throughout this work, I say your patience and attention is deeply appreciated.

I am indebted to my brother, Mr. Benedictus Dotse, my mother, Madam Rita Hortunu and my sister Ernestine Dotse for their financial and moral support throughout my work, I love you all.

Further thanks to Samuel Dedzi, Peter Osei, Daniel Ackom and Dinah Asamoah-Antwi, and to all my friends for their help and supports in various ways.

I am also grateful to Mr. Simon Adzaklo, Dr. Hannah Afum and all who helped me in one way or the other at National Nuclear Research Institute (NNRI) all of the Ghana Atomic Energy Commission.

My final thanks go to all my lecturers, course mates, families and friends who have contributed in one way or the other to bring me this far. God bless us all.

TABLE OF CONTENT

LIST OF FIGURES

LIST OF ABBREVIATIONS

CIP	Carbon in Pulp
CIL	Carbon in Leach
RTD	Residence Time Distribution
CFD	Computational Fluid Dynamics
TKE	Turbulent Kinetic Energy
CSTR	Continuous Stirred Tank Reactor
RRF	Rotating Reference Frame
MRF	Multiple Reference Frame
MRRF	Multiple Rotating Reference Frame
MMRF	Multiple Moving Reference Frame
SRF	Single Reference Frame
2D	2-Dimensional
3D	3-Dimensional
RSM	Reynolds Stress Model
SM	Sliding Mesh
SMM	Sliding Mesh Model
RANS	Reynolds Average Navier-Stokes
URANS	Unsteady Reynolds Average Navier-Stokes
DPM	Discrete Phase Model
VOF	Volume of Fluid
MPM	Mixing Plane Model
RNG	Renormalization Group
SDE	Stochastic Differential Equation
SIMPLE	Semi-Implicit Method for Pressure Linked Equation

PC-SIMPLE	Phase Coupled Semi-Implicit Method for Pressure Linked Equation

ABSTRACT

The numerical method of modelling and simulation was used to model the mixing performance in a stirred tank reactor. In spite of the great advances with which the field of the design of chemical reactors has moved, mixing is poorly understood and the design is generally unsophisticated. For this matter, the objective of the investigation is to characterize the flow field generated within the tank, analyse the degree of mixing and to relate the k-ε turbulent models. Several mathematical models like equations of continuity and momentum equations have been used in the simulation. The hydrodynamic behaviour was understood by velocity magnitude, the radial and axial velocities the volume fractions and the eddy viscosity plots. Eulerian-Eulerian multi-fluid model was simulated using the Eulerian-Eulerian multi-fluid model where the RANS standard k-ε model, RNG k-ε model and the Realizable k-ε model with a multiple reference frame approach were used to model the various parameters. Contours of eddy viscosity show the degree of mixing in the stirred tank. From the results, it can be observed that the standard k-ε and the realizable k-ε gave a uniform plot of eddy viscosity with standard k-ε being the best model and the RNG k-ε model producing a poor eddy viscosity plot. The velocity vector and contour plots were also simulated to determine the flow field in the stirred tank. The standard k-ε shows a better flow field than both the realizable and the RNG k-ε models. The standard k-ε gave a better results when compared.

CHAPTER ONE

INTRODUCTION

The Introductory Chapter presents the background to the study and the basis under which the research was conducted. The research problem statement, relevance and justification of the study is presented in this Chapter together with the Objectives and scope of the study. The final Section of this Chapter presents the outline of the Thesis.

1.1. BACKGROUND TO THE STUDY

There are many factors that determine the value of chemical products. These factors range from quality of raw materials, processing time, storage, process operations etc. The process operations include fermentation, sedimentation, mixing etc. The central determinant of the factors that affects the quality of chemical products especially in the gold mining industry is mixing.

Mixing is the process of reducing inhomogeneity in two or more substances. This inhomogeneity can be in terms of temperature, concentration or phase. The goal of every industry regarding mixing is to obtain a homogeneous fluid or substance (mixture) in shortest time possible (Kars-jordan and Hiltunen, 2007). The worth of the mix determines the worth of the finishing product. Secondary effect such as mass transfer, reaction and product characteristics are usually the critical objective of mixing. Reaction rate and product distribution can be affected by inadequate mixing and mass transfer. In 1989, the cost of poor mixing was estimated at $1billion to $10 billion in the U.S. chemical industry alone (Muzzio, et al., 2004). Combination of three physical processes describe the factors that are important in mixing. These physical processes are the distribution, the dispersion and the diffusion processes.

The process whereby materials are transported to all regions of the vessel by bulk circulation currents is called the distribution process. Also, the process of breaking up bulk flow into smaller eddies is called dispersion. Finally, the random wandering of molecules or atoms as they are pushed to and fro by little random agitations of the neighbors is called diffusion and it can mix up different chemicals on small scales.

The mechanism of fluids fall essentially into four categories: bulk transport, turbulent flow, laminar flow and molecular diffusion (Bhatt and Agrawal, 1980).

Bulk transport first of all, is the movement of a moderately large portion of the material being mixed from one position in the system to another. A simple circulation of material in a mixer may not necessarily result in efficient mixing. Turbulent mixing on the other hand is the phenomenon of mixing which is a direct result of turbulent fluid flow. It can be categorized by random disparity of the fluid velocity at any given point within the system. When highly viscous liquids are being handled, laminar mixing or laminar flow is also regularly faced. It can also happen if stirring is moderately calm and may exist next to stationary surfaces in vessels in which the flow is principally turbulent. Finally, molecular diffusion is the primary mechanism accountable for mixing at the molecular level. When it comes in conjunction with laminar flow, molecular diffusion tends to reduce the sharp gaps at the interface between the fluid layers, and if allowed to proceed for sufficient time, results in complete mixing (Bhatt and Agrawal, 1980).

Mixing can be induced by four factors. These are the nature of the product, the particle size, the particle shape and the particle charge.

The nature of particles contribute to the mixing of substances in one way or the other. Rough surfaces of particles do not bring about good mixing because, active substances may enter into the pores of the other components. A particle that can adsorb on surfaces

can decrease combination during mixing. Particle size variation on the other hand leads to separation as the small particles move downward through the spaces between the bigger particles. As the particle size rises, flow properties also increases due to the effect of gravitational force on the particle size. Also, the shape of particle is a factor to proper mixing. Particles should be spherical in shape for uniform mixing. The irregular shaped particles have less probabilities of separation once they are mixed together because they can become inter-locked. Some particles employ attractive forces due to the electrostatic charges on them. This is called particle charge which is a factor that affect the mixing of substances and also results in separation or segregation (Bhatt and Agrawal, 1980).

The fundamental equipment that aids in mixing are the baffles, the stirred tank reactors, the impellers and other tank internals. Impellers first of all are used to increase or reduce the pressure and flow of a fluid. Impellers can be categorized as either axial, radial or mixed flow depending on the route of the flow through the impeller relative to the axis of rotation. In the case of radial flow impellers, fluids enter in a plane parallel to the axis of rotation or radially outwards towards the vessel and is discharged at 90° to it. They are best used in translational and turbulent regimes and also good for dispersing of liquids. On the other hand, axial flow impellers receive and discharge fluid in a plane parallel to the axis of rotation i.e. it discharges fluid axially towards the base depending on rotational direction. Similar to radial flow impellers, axial flow impellers are also good for transitional and turbulent regimes and also for blending and suspending. The radial and axial flow impeller phenomenon combine to form the mixed flow impellers. Such impellers receive fluid in a plane parallel to the axis of rotation and discharge it at an angle that is between 0 and 90° to the axis of rotation (Yusof et al.,2014). Baffles are flow directing or hindering vanes or panels used in some industrial process vessels

or tanks. The principal aim of baffling is to convert swirling motion into a preferred flow pattern to accomplish process objective of mixing. In stirred vessels, the existence of baffles is important to convert the vortexing motion of the impeller into top to bottom mixing to improve mechanical stability (Myers et al., 2002). Furthermore, stirred tank reactors (or vessels) are commonly used in chemical processing, mineral processing, wastewater treatment plant and various other industries. They are among the most commonly used pieces of equipment in the chemical industry (Khorkpor et al., 2004). They can be categorized as batch, semi-batch or continuous by way of operation or either as isotherm or adiabatic by way of thermal operation (Molnár et al., 2013). The quality of materials mixed in a stirred tank depends on the layout and operating conditions of the tank. The ideal design of a stirred tank for minimum resources and running costs depends on the desired production rate with a specified product's properties and it is achieved by a correct choice of tank and impeller geometry, rotational speed and location of fluid addition and subtraction (Ferreira and Trierweiler, 2009). Mixing is often accomplished in tanks, reactors or mixing apparatuses. Mixing equipment design must go beyond mechanical and costing considerations, with the primary aim being the best to achieve the key mixing process. The equipment that aid mixing in industries are grouped according to the type of material that is being mixed. In the mining industry, mixing takes place in a stirred or an adsorption tank.

To agitate in leaching, neutralization, scrubbing, and replacement and purification process of wet gold melting all take place in a stirred tank. This tank recovers 85% of gold from the ore when effective mixing take place. The crushed ore is fed to the tanks of cyanide solutions, where the gold is dissolved in the cyanide solution.

The parameters that affect the quality of mixing in an adsorption tank are the volume of the adsorption tank, the flow rate, the concentration of the feed (slurry), reaction kinetics, temperature, pressure and residence time distribution (RTD).

Computational fluid dynamics (CFD) is a computer-based tool for simulating the behaviour of systems concerning fluid flow, heat transfer and other associated physical processes. It works by solving the equations of fluid flow over a region of interest with indicated boundary conditions of the region. CFD is typically aimed at resolving selected forms of the Navier-Stokes equations. This can be done by splitting the fluid region into series of control volumes and applying the finite volume method. CFD is an attractive option whenever numerous design disparities are to be analyzed. It is also useful wherever physical investigation may be barred due to restricting factors, such as procedures, scale, cost, accessibility or the presence of physical or environmental hazards. CFD is especially common and most useful in cases where modelling methodologies have been previously validated or operational data or authentication is easily accessible. It has also been confirmed to be a useful tool exactly for industrial combustion employment, and it is routinely applied in the design of combustion equipment. It is used in the design and optimization of air ducts and sessions to ensure airflow in properly distributed to and within combustion equipment. It is also useful for forecasting combustion behavior as well as evaluation of pollutant discharges (Anderson and Londerville, 2013). The residence time distribution describes the mixing and flow within reactors and to relate the behavior of real reactors to their ideal models. It is also used for troubleshooting existing reactors and in estimating the yield of a given reaction and designing future reactors.

1.2. RESEARCH PROBLEM STATEMENT

Despite the widespread use of stirred tank reactors, their fluid dynamics is extremely complex and not adequately understood (Khorkpor et al., 2004). The flow in stirred vessels equipped with baffles is strongly three dimensional and the complexities are not taken into consideration at the design stage. This is one main reason for the failure of most stirred vessels.

Inadequate understanding of mixing operation, in general, is partly due to the methods used to analyze the flow dynamics in mixing vessels. Flow dynamics of stirred vessels with different impeller types and vessel geometries have been investigated using experimental approaches such as residence time distribution (RTD) technique. Even though it is considered the best experimental technique, the RTD methodology is not only costly to conduct but also incapable of providing pictorial information, such as mixing zones and velocity fields of impellers, that are needed at the design stage.

There is therefore the need for research using techniques that can provide such information which is very essential for process unit design.

1.3. RELEVANCE AND JUSTIFICATION

The fundamental knowledge of the hydrodynamics such as the velocity and turbulent kinetic energy (TKE) distributions in stirred tanks is very useful for improving engineering design as well as evaluating practical performance (Devi and Kumar, 2012a). An appropriate design model for such mixing tanks requires information of various transport, kinetic and mixing parameters which can be modelled using CFD (Devi and Kumar, 2012b). Mass concentration, velocities and flow variables can best be described by CFD modelling with details anywhere in the flow region not usually

available through experiments. Furthermore, adequate information on mixing tank hydrodynamics is essential for improvement of both unit operational cost and product quality.

Usually, in industrial circumstances, vessels are made of non-transparent substances, the operating liquids are opaque and essential gassing rates are high, all of which suggest complications for experimental measurement of turbulent flow fields in such vessel kinds. For these reasons, CFD modelling is the ideal tool for the prediction of flow fields in industrial vessels to better understand flow phenomena (Aubin et al 2004).

1.4. OBJECTIVES

The main objective of the study is to employ CFD to model the mixing zones in a stirred tank.

To achieve the main objective, the following specific objectives will be pursued:

1. Model the flow field (velocity and eddy viscosity) in the stirred vessel using CFD
2. Analyse the degree of mixing in the tank using eddy viscosity
3. Compare the various $k-\varepsilon$ turbulent models

1.5 SCOPE OF THE STUDY

To overcome the research problem, the flow field of the adsorption tank was simulated and determined. This work is purely numerical using Computational Fluid Dynamics (CFD) approach. This would provide pictorial information and to understand complex fluid dynamics. Experimental procedure was not considered in this work.

1.6. OUTLINE OF RESEARCH

The research work was focused on determining the flow field in a Stirred Tank using CFD.

The whole study was organized into five Chapters. Chapter one presents the introduction of the thesis consisting of an overview to the Chapter, background to the study, problem statement, goal and objectives of the study. It continues with the relevance and justification of the research and conclusion to the Chapter.

The second Chapter focuses on detailed literature review or survey on determining the concept of mixing, mixing equipment and the degree of mixing. Furthermore, the laminar flow and the governing equation for Multiphase flow using CFD was also presented in this Chapter. Also, flows in the Rotating and Multiple Reference frame were presented with their equations. The various turbulent models were also outlined in this chapter.

In Chapter three, the research methodology includes the drawing and meshing of the geometry, solving the geometry and modelling equations of continuity and momentum for turbulent flows. ANSYS FLUENT software was used as the computational tool.

Also, the result in the form of contour and vector plots were analysed and discussed in Chapter four. Finally, in Chapter five, summary of the major findings, conclusions, recommendations and suggestions for future study was presented.

CHAPTER TWO

LITERATURE REVIEW

In this chapter, the general explanation on mixing, mixing operations, mixing equipment and the degree of mixing are outlined. Furthermore, the literature on the application of CFD in CSTR analysis is also outlined with laminar flow model and flows with rotating reference frame. The various models, multiple reference frame, turbulent flow including their various forms of mathematical equations are thoroughly reviewed.

2.1. CONCEPT OF MIXING

Mixing of fluids in tanks is an important aspect of many chemical processing operations and can occur either by laminar or turbulent flows. It is the combination of two or more substances to form one substance or mass, and the quality of the final product and its attributes are derived from the quality of the mix.

The objective of every mixing is homogenization, establishing itself in a reduction of concentration or temperature gradients or both simultaneously within a mixing reactor, (Prasanna et al., 2016). In homogenization, the equalization of concentration and temperature differences is the most important and the most frequently carried out mixing operation. Furthermore, enhancing heat transfer between a liquid and heated surface which is another mixing operation reduces the thickness of the liquid boundary layer. Hence the thermal resistance on the heat transfer surface and convective motion of the tank contents to ensure that the temperature gradients within the tank content are reduced. Also, suspension of solid in a liquid is a homogeneous distribution of the solid in the bulk of the liquid. Through efficient mixing, settling of the particles suspended in the liquid as a result of gravity is prevented. This is an important phenomenon in

gold leaching tanks for example where the desire is to have the solids suspended off the bottom of the tank in order to have higher efficiency of gold recovery.

Mixing inclines to being a simple issue in turbulent flows, where random velocity fluctuations can bring about rapid homogenization. On the contrary, in laminar flows, a universally uniform end result is far from guaranteed. Laminar conditions are inevitable if the fluids involved are very viscous or shear-sensitive. Inadequate mixing results in a homogeneous material that lacks consistency with respect to anticipated characteristics such as chemical composition, colour, texture, flavour, reactivity and particle size (Holloway et al., 2012).

Mixing operations may involve single-phase liquid mixing , liquid-liquid mixing, solid-liquid mixing, gas-liquid mixing, solid-solid mixing and in some instances three-phase mixing involving solid, liquid and gas. The mixing requirements depend on the processes used. The requirements for liquid-liquid mixing are very different from those of liquid-solid or liquid-gas mixing, (Pordal and Matice, 2003). A vital mixing operation involves bringing diverse molecular species together to achieve a chemical reaction. In some cases, temperature alteration exist between an equipment surface and the bulk fluid, or between the suspended particles and the continuous phase fluid, (Coker, 2001).

2.2. MIXING EQUIPMENT

Equipment that aid mixing are the mixing vessels, the impellers and baffles. The principal purpose of a mixing vessel is to provide adequate stirring and mixing of the fluid. The mixing characteristics influence the product worth and competence of the procedure to a great degree. Mixing or stirred vessels come in different shapes and sizes. The main vessel is cylindrical in shape and the vessel bottom is most often

contoured. Mixing of fluids occurs in several types of vessels and tanks with different geometrical shapes and sizes (Rabiner and Gold, 1985). The top of the vessel may be opened or sealed. The bottom of the vessel is normally not flat but rounded to abolish sharp corners or regions into which the fluid currents would not penetrate. Dished ends are most common. The height of the tank is approximately equal to the diameter of the tank. To enhance mixing, an impeller is normally mounted on a shaft supported above the tank to impart motion and shear to the fluid (i.e. agitation).

Furthermore, an important component of a stirred tank is the agitator or impeller. The rotating impeller imparts motion and shear to the fluid thus inducing mixing. The type of impeller engaged depends on the nature of the task (Pordal and Matice, 2003). Agitation plays a vital role in the success of many chemical processes, and there is wide range of commercially accessible impellers that can provide the optimum degree of mixing for any process. The difficulty arises when selecting the best impeller for the required process. The process objective of an impeller is the primary factor that determines its selection. Impellers can be classified into two groups depending on the size of blade of the impeller. These are impellers with a small blade area, which rotate at high speeds, examples include turbines and marine propellers, and impellers with large blade area, which rotate at low speeds. These include anchors, paddles and helical screws. Impellers with large blade area are very effective for high viscosity liquids and depend on area to produce liquid movement throughout the vessel. Since they are low-shear impellers, they are useful for mixing shear-thickening liquids (Cheremisinoff, 2000). Impellers are broadly classified as axial or radial flow impellers. Axial flow impellers cause the fluid to flow parallel to the impeller's rotation axis. On the other hand, radial flow impellers cause the fluid to flow perpendicular to the impeller's rotation axis (Gurmen, 2008).

Also, the tank may also contain baffles which are flow directing vanes. Baffles are included in the vessel to break the vortex and prevent solid body rotation of the fluid. The primary purpose of baffling is to convert swirling motion into a preferred flow pattern to accomplish the process objectives i.e. efficient mixing. Baffles set away from the tank wall create turbulence and thus, improve the entrainment of liquid in contact with the wall of the tank.

2.3. DEGREE OF MIXING

A high degree of mixing takes place when the whole liquid mass, confined in a vessel is under turbulent flow condition. High turbulence in a stirred tank generates higher degree of mixing thereby ensuring effective mixing within vessels. The function of the extent of eddy currents or turbulence formed and the forces tending to diminish the formation of eddy currents is the degree of mixing in a system. This relationship may by expressed as

$$\frac{Driving\ force}{Resistance} = Degree\ of\ mixing \qquad (2.1)$$

In this case, the driving force is the force producing eddy current and the resistance is the force tending to dampen the formation of eddy currents (Castro et al,. 2015).

2.4. APPLICATION OF COMPUTATIONAL FLUID DYNAMICS IN CONTINUOUS STIRRED TANK REACTOR (CSTR) ANALYSIS

Computational fluid dynamic (CFD) is a complex numerical method for modelling and simulating fluid flow and chemical processes. CFD can be applied in diverse ways such as in aerospace, aeronautics, automotive, power process industries and in fluid dynamics and can provide 2D as well as 3D views. In this work however, the 3D view

of fluid flow field was applied. Also, parameters such as velocity, temperature, turbulence kinetic energy, eddy viscosity among many others of the flow field can be processed using CFD. CFD is being used in this work because it provides detailed spatial distribution of the flow fields, (Mohd et al., 2013). It also have the capability of predicting the complete velocity in a vessel, therefore provides simpler means of determining the residence time distribution (RTD) apart from the experimental method. The experimental RTD approach detects and characterizes main features of the flow while CFD locates them, which is normally the reason why CFD is used as a complementary tool to the experimental approach.

Middleton *et al*. in 1986 carried out simulation of turbulent flow using standard $k-\varepsilon$ turbulence model. No quantitative comparison of the mean flow and turbulent characteristics were presented. The flow field anticipated was used to study the outcome of mixing on the yield of a typical consecutive. Multiple Reference Frame (MRF) and $k-\varepsilon$ model were used on the other hand to simulate the flow in a stirred tank by Dong *et al*. in 1994. The flow away from the impeller region was well predicted while the magnitudes of axial and radial velocities were overestimated in the near impeller region. The turbulent kinetic energy was over predicted in the impeller stream.

The standard $k-\varepsilon$ in which the species concentration associated with turbulent flow was calculated in terms of its turbulence kinetic energy and dissipation rate via Finite rate/Eddy dissipation model by Udaya et al. in 2003. There was a very good agreement between the experimental values and simulation results.

Simulation of flow in a stirred tank was also done by Yoon et al. in 2000 using 2D and 3D Reynolds-averaged Navier- Stokes equation. In the rotating frame, the model for the impeller induced velocity field appears as a steady boundary condition. Comparing the 3D simulation to the experimental, showed a qualitative agreement between them.

Even so, the results of Reynolds- averaged simulations quantitatively differ from the experimental measurements. Furthermore, Yeoh et al., in 2004 simulated turbulent flow characteristics in a stirred vessel using large eddy simulation and Reynolds Averaged Navier-Stokes approaches with the sliding or deforming mesh method. The results were compared with the detailed experimental data of mean and root mean square (rms) velocities and energy dissipation. It was also observed that there was a very good qualitative and quantitative agreement between the large eddy simulation predictions and the measured data.

Also, Standard $k-\varepsilon$ model and the Multiple Reference Frame (MRF) were used by CAO et al. in 2008 to simulate the fluid dynamics in a tubular stirred reactor. Under the effect of agitation, the distribution of velocity showed the flow field was turbulent. The RTD curves predicted with CFD also showed good agreement with experimental data. Additionally, the standard $k-\varepsilon$ model and the Reynolds Stress model (RSM) were used in a simulation done by Huang and Li in their 2006 simulation work predicted the momentum source term without the help of experimental data. So the momentum source term approach for CFD prediction of the impeller propelling action was developed as a tool with predictive capacity. It was also observed that the numerical comparisons of flow field showed that the momentum source term approach predictions were in good agreement with the experimental data. It was also found that the prediction accuracy of momentum source term approach was better and with the least computational approach than the Multiple Reference Frame (MRF) and Sliding Mesh (SM).

Similarly, a three dimensional URANS simulations of flow and entrainment processes in a jet-mixed tank was simulated by Marek et al. in 2002. The predicted mixing time and concentration profile were compared to experimental measurements for different

jet velocities and nozzle angles. Also from the result, the numerical model predicted the overall mixing time very well. However, apart from on probe location, the predicted concentration profiles were generally not in good agreement with the experimental measurements. It was also shown that the convection scheme can have an effect on the tracer distribution and that improvements were accomplished in comparison to the CFD results from literature.

Lee et al. in 1996 used sliding mesh (SM) technique to simulate the impeller rotation. It was observed that the turbulent kinetic energy was severely under predicted (maximum deviation 200%). Instantaneous radial velocity was over predicted in most of the regions with maximum departure of 35% from experimental data.

Additionally, Rigby et al. 1997 also employed Sliding Mesh technique to simulate the action of rotating impeller. Reasonable agreement with the experimental data for the location of impeller was observed. Comparison of all the three velocity components showed slight under predictions in the impeller centre plane and slightly above the impeller.

More so, two-dimensional model for the prediction of flow pattern in stirred vessel were also proposed by Kuncewicz et al. 1997. Poor tangential velocity prediction (maximum deviation 100%) was observed while the axial velocity agreed reasonably well.

Venneker and Van den Akker, 1997 also attempted the simulation of the flow using the black box approach along with the $k-\varepsilon$ turbulence model. The computed radial velocities agreed well throughout the tank while axial velocity predictions were satisfactory in most of the region (under predicted by as much as 50% below the impeller). The turbulent kinetic energy predictions were good except near the shaft and the bottom of the impeller where they were severely under predicted.

CFD simulations were likewise carried out by Brucato et al. 1994 of the flow in stirred tanks using various impeller models, namely black box approach, inner-outer technique and sliding grid approach along with the standard $k-\varepsilon$ turbulence model. Alternative modelling approaches were also compared.

Tabor et al., 1998 made use of the MRF approach and the sliding mesh (SM) approach. The standard $k-\varepsilon$ turbulence model was used to model the turbulence. They recommended Multiple Reference Frame (MRF) for low diameter to height ratio of the tank, and suggested its inapplicability for the small blade-baffle gap and the cases where the time dependent features are of importance.

Montante et al., 1999 carried out simulations to study the effect of impeller clearance on the prediction of flow patterns. The clearance ratio was modeled from 0.12 to 0.33. Three different turbulence models were used. These were the standard $k-\varepsilon$ model, the renormalization group (RNG) $k-\varepsilon$ model and the Reynolds Stress Model (RSM). The impeller-baffle interaction was modelled using Sliding Mesh (SM) and inner-outer approach. They reported the velocity vector plots to show the clearance effect on number of circulation loops.

Turbulent flow field was also simulated by Alcamo et al., 2005 using Large Eddy Simulation in an un-baffled stirred tank, stirred by Rushton turbine. The Smagorinsky model was used to model sub-grid scales. The simulated results were compared with experimental data and they formed an excellent agreement especially for mean tangential velocities.

Mixing studies were carried out using CFD as well as experiments by Javed et al., 2006 in eight different locations in bulk and impeller region as concentration measurement locations were considered. The mean axial, tangential and radial velocities were

comparatively reported and the simulation results were observed to be in very good agreement with the experimental data.

Xiao-chang et al., 2009 also worked on the RTD study on a new tubular shaped continuous reactor using number of tee type impeller supported on a coaxial shaft. They performed both the experimental work and theoretical analysis by Fluent 6.3. The tracer was injected as a pulse input in the experimental analysis. The characteristics of experimental RTDs were predicted well by fluent at different speeds of the impeller and at different inlet flow rates. It was observed that the tubular reactor with a stirrer can improve the flow profile by narrowing the RTD curve, decreasing mean residence time and avoiding back mixing, but a high stirring speed broadens the RTD curve drastically. As the flow rate increases, the mean residence time as well as the variance of RTD was found to decrease proportionally. As the rotation speed increases, no evident effect on the mean residence time was observed, whereas the variance got enlarged greatly.

Rajavathsavai et al., 2013 used CFD to study the change of fluid flow behaviour inside the reactor either from dispersion to ideal or ideal to dispersion mixing state. The mixing behaviour was predicted in terms of age distribution function I(θ). For the CSTR with or without impeller and baffles, I(θ) was found by the tracer injection method. This was measured and predicted by impeller swept volume method. The predicted results were found to be in good agreement with experimental data.

The Residence Time Distribution determines any malfunctions in a stirred tank but cannot show the visual image of the flow field. Therefore numerical approach is used in this work to determine the flow field and also determine the Residence Time Distribution using the Computational Fluid Dynamics (CFD) which is presented in the next section.

2.5. CFD MODELLING OF MULTIPHASE FLOWS

Computational fluid dynamics (CFD) can be used to comprehensively model a wide range of incompressible and compressible, laminar and turbulent fluid flow problems. In CFD analysis, a broad range of mathematical models for transport phenomena is combined with the ability to model complex geometries, for example modelling of multiphase flows in bubble columns and mixing in stirred tank reactors. To permit modelling of fluid flow and related transport phenomena in industrial equipment and processes, various useful features are provided. For flows involving particle tracking, a discrete phase model (DPM) can be performed. The DPM performs Lagrangian trajectory calculations for dispersed phases (particles, droplets, or bubbles), including coupling with the continuous phase. For industrial equipment and processes that involve moving and stationary parts, CFD provides the options to model moving and stationary reference frames. The moving reference frame family of models includes the ability to model single or multiple reference frames. Robust and accurate turbulence models are a vital component of CFD analysis involving fluid flow (Ansys Fluent, 2012). Turbulence models provide a broad range of applicability, and include the effects of other physical phenomena, such as buoyancy and compressibility.

In this thesis, the focus is on determining the effect of mixing and Residence Time Distribution (RTD) in a stirred tank using CFD. The stirred tank which is isothermal has made it possible for isothermal systems to be chosen, and hence, only the continuity and the momentum equations are solved depending upon the flow regime, (laminar or turbulent flow). ANSYS fluent version 14.5 was used for the simulation study of mixing and RTD on a stirred tank. In the next Section, the theoretical background and the

required CFD model equations are presented based on the ANSYS fluent theory manual (FLUENT, 2009) and from literature.

2.5.1. LAMINAR FLOW MODEL

Laminar flow occurs when a fluid flows in parallel layers, with no disruption between the layers and no cross current or eddies are perpendicular to the direction of flow. Mixing occurs in molecular levels between layers. Laminar flow is referred to as streamline or viscous flow.

The general equation for the conservation of mass or continuity can be written as

$$\frac{\partial \rho}{\partial t} + \nabla \cdot (\rho \vec{v}) = S_m \qquad (2.2)$$

where $\vec{v}$ is the velocity vector and S_m is the source term (i.e. mass added to the continuous phase from the dispersed second phase).

The conservation of momentum equation in an inertial reference frame is given by

$$\frac{\partial}{\partial t}(\rho \vec{v}) + \nabla.(\rho \vec{v}\vec{v}) = -\nabla p + \nabla.\left(\overline{\overline{\tau}}\right) + \rho \vec{g} + \vec{F} \qquad (2.3)$$

where p is the static pressure and $\left(\overline{\overline{\tau}}\right)$ is the stress tensor, $\vec{g}$ and $\vec{F}$ are the gravitational and external body forces respectively. The stress tensor $\left(\overline{\overline{\tau}}\right)$ in equation (2.6) can be expressed as

$$\overline{\overline{\tau}} = \mu\left[\left(\nabla \vec{v} + \nabla \vec{v}^{T}\right) - \frac{2}{3}\nabla.\vec{v}I\right] \qquad (2.4)$$

where μ is the molecular velocity, I is the unit tensor.

2.5.2. GOVERNING EQUATIONS FOR MULTIPHASE FLOWS

A multiphase fluid is composed of two or more distinct components or phases which themselves may be fluids or solids and has characteristic properties of a fluid. It is a simultaneous flow of materials with different states or phases. Each of the phases is considered to have separately defined volume fraction which makes the sum to be equal to unity (Hiltunen et al., 2009). In general, a multiphase fluid may be a comparatively uniform mixture of its components or it may be clearly inhomogeneous in macroscopic scale. It is a complex phenomenon which is difficult to understand, predict or model.

For multiphase flows, ANSYS Fluent solves the transport equations for two types of scalars: per phase and mixture. In the per phase method, denoting an arbitrary scaler *k*, in phase-*l*, as Φ_l^k ; the transport equation inside the volume of phase-*l* is solved as

$$\frac{\partial\left(\alpha_l \rho_l \Phi_l^k\right)}{\partial t} + \nabla \cdot \left(\alpha_l \rho_l \vec{u}_l \Phi_l^k - \alpha_l \Gamma_l^k \nabla \Phi_l^k\right) = S_l^k \qquad \boldsymbol{k=1,\ldots,N} \qquad (2.5)$$

where α_l, ρ_l and u_l are the volume fraction, physical density and velocity of phase-*l* respectively. Γ_l^k and S_l^k are the diffusion coefficient and source term respectively in phase-*l*. In this case, scalar Φ_l^k is associated only with one phase (phase-*l*) and is considered an individual field variable of phase-*l* (Ansys Fluent, 2012). On the other hand, if the transport variable described by scalar Φ_l^k represents the physical field that is shared between phases, or is considered the same for each phase, then the scaler can be considered as being associated with a mixture of phases, Φ^k . The transport equation for the scalar in the mixture then becomes

$$\frac{\partial\left(\rho_m \Phi^k\right)}{\partial t} + \nabla.\left(\rho_m \vec{u}_m \Phi^k - \Gamma_m^k \nabla \Phi^k\right) = S_m^k \qquad \textbf{k=1,…,N} \qquad (2.6)$$

where mixture density ρ_m, mixture velocity u_m and mixture diffusivity for the scalar k Γ_m^k are calculated by

$$\rho_m = \sum_k \alpha_l \rho_l \qquad (2.7)$$

$$\rho_m \vec{u}_m = \sum \alpha_l \rho_l \vec{u}_l \qquad (2.8)$$

$$\Gamma_m^k = \sum_l \alpha_l \Gamma_l^k \qquad (2.9)$$

$$S_m^k = \sum_l S_l^k \qquad (2.10)$$

To calculate mixture diffusivity, individual diffusivities for each material associated with individual phases must be specified (FLUENT, 2009).

There are different improved models that can account for different levels of information, meaning different levels of accuracy and are suitable for different multiphase flow applications. Some of the modelling approaches are the Euler-Lagrange approach, the Euler-Euler approach, the Volume of Fluid (VOF) model and dispersed phase modelling (Stenmark, 2013).

2.5.2.1 EULER-LAGRANGE APPROACH

The Lagrangian discrete phase model in ANSYS FLUENT follows the Euler-Lagrange approach. In this approach, particles are treated as a continuum by solving the Navier-Stokes equation. The particles are tracked on the level of a single particle where the

particle refers to either a solid particle or a gas/fluid bubble/droplet. Conservation equations are solved for the continuous phase and the particle phase is tracked by solving the equations of motion for each particle as shown below.

$$\frac{\partial \alpha_f \rho_f}{\partial t} + \nabla.\left(\alpha_f \rho_f u_f\right) = S_m \qquad (2.11)$$

$$\frac{\partial \alpha_f \rho_f}{\partial t} + \nabla.\left(\alpha_f \rho_f u_f u_f\right) = \alpha_f \nabla p - \alpha_f \nabla.\tau_f - S_p + \alpha_f \rho_f g = 0 \qquad (2.12)$$

$$\frac{\partial u_p}{\partial t} = \sum F \qquad (2.13)$$

Here, α is volume fraction, S_p momentum source term existing in case of exchange of momentum between the phases and F is force. The subscripts *f* and *p* refers to the fluid and particle phases respectively.

The forces acting on particles vary depending on the flow situation. The drag force, lift force, turbulence dispersion force, virtual mass force and/or history force among others are the forces available in the model. When performing numerical modelling, it is up to the modeler to judge which force that are of importance to the flow situation. Adding more forces to a model increases accuracy but also increases complexity. Coupling between the continuous phase and the dispersed phase is achieved through the source terms.

2.5.2.2 EULER-EULER APPROACH

In Euler-Euler models, all phases are treated as continuous and so for this reason, the models are often called multi-fluid models. The Euler-Euler approach can also be used

to model dispersed flows when the overall motion of particles is of interest rather than tracking individual particles. The dispersed phase equations are averaged in each computational cell to achieve mean fields. To be able to describe the dispersed phase as a continuum, the volume fraction should be high and hence this approach is suitable for dense flows.

The phases are treated separately and one set of conservation equations are solved for each phase. Coupling between the phases is achieved through a shared pressure and interphase exchange coefficients. The interphase exchange coefficients need to be modelled. In addition to the regular transport equations, a transport equation for the volume fraction is also solved for each phase. The governing equations for a two-fluid model with two continuous phases are shown below.

$$\frac{\partial \alpha_k \rho_k}{\partial t} + \nabla.\left(\alpha_k \rho_k u_k\right) = 0 \qquad (2.14)$$

$$\frac{\partial \alpha_k \rho_k u_k}{\partial t} + \nabla.\left(\alpha_k \rho_k u_k u_k\right) = -\alpha_k \nabla \mathrm{P} + \alpha_k \nabla.\tau_k + \alpha_k \rho_k g_k + S_k = 0 \qquad (2.15)$$

$$\frac{\partial \alpha_k}{\partial t} + \nabla.\left(\alpha_k u_k\right) = 0 \qquad (2.16)$$

Here, *u* is the mean velocity field and P is the mean pressure shared by the phases. The subscript k refers to the kth continuous phase.

2.6. MODELLING FLOWS WITH ROTATING REFERENCE FRAMES

Fluid flow and heat transfer by default are solved in a stationary reference frame using ANSYS FLUENT (Ansys Fluent, 2012). There are however, many problems in which solving the equation in moving reference frame can be of advantage. Such problems typically involve moving parts such as rotating blades, impellers and similar types of moving surfaces, and it is the flow around these moving parts that is of interest. The moving reference frame models, the flow around the moving part as a steady-state problem with respect to the moving frame. It is possible for many problems to refer to an entire computational domain to a single moving reference frame or single reference frame (SRF) approach. For more complex geometries, it may not be possible to use a SRF. In complex cases, the problem must be divided into multiple zones, with a well-defined interface between the zones. For complex geometries, there are two approximate steady-state modelling methods for this class of problem. These are the multiple reference frame (MRF) approach and the mixing plane approach (Ansys Fluent, 2012).

2.6.1 EQUATION FOR A ROTATING REFERENCE FRAME

Considering a coordinate system that is translating with a linear velocity $\vec{v}_t$ rotating steadily with angular velocity $\vec{\omega}$ relative to a stationary reference frame, the axis of rotation can be defined by a unit direction vector $\hat{a}$ such that

$$\vec{\omega} = \omega \hat{a} \tag{2.17}$$

The computational domain for the CFD problem can be defined with respect to the rotation frame such that an arbitrary point in the CFD domain is located by a position vector $\vec{r}$ from the origin of the rotating frame. The fluid velocities can then be

transformed from the stationary frame to the rotating frame using the following relations

$$\vec{\upsilon}_r = \vec{\upsilon} - \vec{u}_r \tag{2.18}$$

where $\vec{u}_r$ can further be expressed as

$$\vec{u}_r = \vec{v}_t + \vec{\omega} \times \vec{r} \tag{2.19}$$

In equation 2.18, $\vec{\upsilon}_r$ is the relative velocity (the velocity viewed from the moving frame), $\vec{\upsilon}$ is the absolute velocity (the velocity viewed from the stationary frame) and $\vec{u}_r$ is the "whirl" velocity (the velocity due to the moving frame).

When the equations of motion are solved in the moving reference frame, the acceleration of the fluid is augmented by additional terms that appear in the momentum equations, (Batchelor, 1967). These equations can be formulated in two different ways:

i. The momentum equations are expressed using the relative velocities as dependent variables (known as the relative velocity formulation).
ii. The momentum equations are expressed using the absolute velocities as dependent variables in the momentum equations (known as the absolute velocity formulation).

2.6.2. FLOWS IN MULTIPLE REFERENCE FRAMES

Many problems involve multiple moving parts or contain stationary surfaces which are not surfaces of revolution and therefore cannot be used with Single Reference Frame modeling approach. For such problems involving both moving and stationary zones, the model is broken up into multiple fluid/solid cell zones, with interface boundaries separating the zones (Ansys Fluent, 2012). In this way, zones containing the moving components can be modelled using the moving reference frame equations whereas

stationary zones are modelled with the stationary frame equations. The manner in which the equations are treated at the interface lead to two approaches. These are the Multiple Moving Reference Frames (MMRF) and Sliding Mesh Model (SMM). The Multiple Reference Frame Model (MRF) and the Mixing Plane Model (MPM) are the two types of MMRF. Both the MRF and the mixing plane model are steady-state approximations and differ primarily in the manner in which conditions at the interfaces are treated.

2.6.2.1. THE MULTIPLE REFERENCE FRAME MODEL

The MRF model is a steady-state approximation in which individual cell zones can be assigned different rotational and/or translational speeds. The flow in each moving cell zone is solved using the moving reference frame equations and if the zone is stationary, the equations reduce their stationary forms. The MRF approach does not account for the relative motion of a moving zone with respect to adjacent zones which may be moving or stationary (FLUENT, 2009).

The interface treatment applies for the velocity and velocity gradients, since these vector quantities change with a change in reference frame. Scalar quantities such as temperature, pressure, density, turbulent kinetic energy, etc. do not require any special treatment, and thus are passed locally without any change. At the interface the discretized diffusional terms in one domain require the values for velocities in other domain.

When relative velocity formulation is used, velocity in each subdomain is calculated relative to motion of subdomain. The conversion equation from relative velocity to absolute velocity is given as:

$$\vec{\upsilon} = \vec{\upsilon}_r + (\vec{\omega} \times \vec{r}) + \vec{\upsilon}_t \qquad (2.20)$$

where, $\vec{\upsilon}_t$ is the translation velocity.

From equation (2.13), the gradient of absolute velocity vector can be shown to be

$$\nabla \vec{\upsilon} = \nabla \vec{\upsilon}_r + \nabla(\vec{\omega} \times \vec{r}) \tag{2.21}$$

When absolute velocity formulation is used, the governing equations in each sub-domain are solved with respect to that sub-domain's reference frame, but the velocities are stored in the absolute frame. Therefore, no special transformation is required at the interface between two sub-domains. Though the MRF approach is an approximation, it can provide a reasonable model of the flow for many applications (Ansys Fluent, 2012). For example, in mixing tanks, since the impeller-baffle interactions are relatively weak, large-scale transient effects are not present and the MRF model can be used. Another potential use of the MRF model is to compute a flow field that can be used as an initial condition for a transient sliding mesh calculation.

2.6.2.2. THE MIXING PLANE MODEL

The mixing plane model provides an alternative to the multiple reference frame and sliding mesh models for simulating flow through domains with one or more regions in relative motion. The essential idea behind the mixing plane concept is that, each fluid zone is treated as a steady-state problem. Data from the flow-field from adjacent zones are passed as boundary conditions that are spatially averaged or mixed at the mixing plane interface. Three different types of averaging methods are available when using the mixing plane model: area-weighted averaging, mass averaging, and mixed-out averaging (Ansys Fluent, 2012).

2.6.2.3. THE SLIDING MESH MODEL

The sliding mesh model allows separate zones to move relative to each other. The motion can be translational or rotational. They are separated into two regions that are treated separately. These are the impeller region and the tank region, with the tank region being the bulk of the liquid, the tank wall, the tank bottom and the baffles. The relative motion of stationary and moving components will give rise to temporary interactions. The temporary solution that is required in a sliding mesh simulation is time-periodic (Ansys Fluent, 2012).

2.7. MODELLING TURBULENT FLOW

In turbulent flow, there is increased mixing that results in viscous losses which are generally much bigger than in laminar flow. Turbulence could be thought of as instability of laminar flow that occurs at high Reynolds number (Re). Such instabilities originate from interactions between non-linear inertial terms and viscous terms in Navier-Stokes equation. These interactions are rotational, fully time-dependent and fully three-dimensional. Rotational and three-dimensional interactions are mutually connected via vortex stretching. Vortex stretching is not possible in two dimensional space that is why no satisfactory two-dimensional approximations for turbulent phenomena are available (Oden and Prudhomme, 2002). Furthermore, turbulence is thought of as random process in time and therefore deterministic approach is possible. Another important feature of turbulent flow is that vortex structures move along the flow. Their lifetime is usually very long hence, certain turbulent quantities cannot be specified locally.

2.7.1. REYNOLDS (ESEMBLE) AVERAGING

The Navier-Stokes equations have the capability to solve both laminar and turbulent flows without the need for additional information (ANSYS CFX, 2012). However, this would involve length scales much smaller than the smallest finite volume mesh. To overcome the use of finer mesh to model the effects of turbulence, statistical turbulence models using Reynolds averaging are adopted for practical engineering calculations. In Reynolds averaging, the solution variables in the instantaneous (exact) Navier-Stokes equations are decomposed into the mean (ensemble-averaged or time-averaged) and fluctuating components. For the velocity components:

$$u_i = \bar{u}_i + u_i', \tag{2.22}$$

and

$$p = \bar{p} + p' \tag{2.23}$$

where the mean and fluctuating parts satisfy

$$\bar{u}_i = U_i, \qquad \bar{u}_i' = 0 \tag{2.24}$$

$$\bar{p} = P, \qquad \bar{p}' = 0 \tag{2.25}$$

with the bar denoting time average.

Substituting expressions of this form for the flow variables (i.e. equations 2.24 -2.25) gives Reynolds-averaged Navier-Stokes (RANS) equation. The continuity and momentum equations can be written as:

Continuity equation

$$\frac{\partial \rho}{\partial t} + \nabla . \rho \vec{v}_r = 0 \tag{2.26}$$

Momentum equation

$$\frac{\partial}{\partial t}(\rho \vec{v}_r) + \nabla . (\rho \vec{v}_r \vec{v}_r) + \rho(2\vec{\omega} \times \vec{v}_r + \vec{\omega} \times \vec{\omega} \times \vec{r}) = -\nabla p + \nabla . (\bar{\bar{\tau}}_r) + \rho \vec{g} + \vec{F} \tag{2.27}$$

The momentum equation contains two additional acceleration terms: the Coriolis acceleration ($2\vec{\omega} \times \vec{v}_r$), and the centripetal acceleration ($\vec{\omega} \times \vec{\omega} \times \vec{r}$). The viscous stress, $\bar{\bar{\tau}}_r$ is

$$\bar{\bar{\tau}}_r = \mu \left[\left(\nabla \vec{v} + \nabla \vec{v}_r^{\,T} \right) - \frac{2}{3} \nabla . \vec{v}_r I \right] \tag{2.28}$$

where μ is the molecular viscosity , I is the unit tensor and the second term on the right hand side is the effect of volume dilation.

In equation 2.27, additional terms, the Reynolds stresses, $\bar{\bar{\tau}}_r$ represent the effects of turbulence. These Reynolds stresses must be modeled in order to close equation 2.27. Various models exist to model the Reynolds stresses, such as the $k-\varepsilon$, $k-\omega$, Shear Stress Transport models etc.

In this thesis, the $k-\varepsilon$ model has been used. ANSYS fluent provides three types of $k-\varepsilon$ models which have all been used in this thesis and are presented in the next Section.

2.7.2. STANDARD $k-\varepsilon$ MODEL

The standard $k-\varepsilon$ model proposed by Launder and Spalding in 1972 is the most widely used model because it is robust, economical and has serve the engineering community well for many years (Launders and Spalding, 1972). This model provides rapid, stable calculation and reasonable results for many flows especially those with high Reynold number. It is a semi-empirical model based on the transport model of turbulent kinetic energy (k) and its dissipation rate (ε). The derivation of $k-\varepsilon$ model assumes that the flow is fully turbulent, and the effect of molecular viscosity on the flow is negligible. The model is therefore valid only for fully turbulent flow.

The transport equation for k is expressed as

$$\frac{\partial}{\partial t}(\rho k)+\frac{\partial}{\partial x_i}(\rho k \upsilon_i)=\frac{\partial}{\partial x_i}\left[\left(\mu+\frac{\mu_t}{\sigma_k}\right)\frac{\partial k}{\partial x}\right]+G_k+G_b-\rho\varepsilon-Y_M+S_k \qquad (2.29)$$

and the transport equation for ε is expressed as

$$\frac{\partial}{\partial t}(\rho\varepsilon)+\frac{\partial}{\partial x_i}(\rho\varepsilon\upsilon_i)= \frac{\partial}{\partial x_i}\left[\left(\mu+\frac{\mu_t}{\sigma_\varepsilon}\right)\frac{\partial\varepsilon}{\partial x}\right]+C_{1\varepsilon}\frac{\varepsilon}{k}(G_K+C_{3\varepsilon}G_b)-C_{2\varepsilon}\rho\frac{\varepsilon^2}{k}+S_\varepsilon \qquad (2.30)$$

where μ_t is the turbulent viscosity, G_K is the generation of turbulence kinetic energy due to the mean velocity gradients, G_b is the generation of turbulence kinetic energy due to buoyancy, Y_M represents the contribution of the fluctuation of the fluctuating dilation in compressible turbulence to the overall dissipation rate, $C_{1\varepsilon}$, $C_{2\varepsilon}$, and $C_{3\varepsilon}$ are constants,

σ_ε and σ_k are the Prandtl numbers for ε and k respectively, S_k and S_ε are user-defined source terms.

The turbulent or eddy viscosity μ_t can be calculated by combining k and ε as follows:

$$\mu_t = \rho C_\mu \frac{k^2}{\varepsilon} \tag{2.31}$$

where C_μ is constant.

The model constants $C_{1\varepsilon}$, $C_{2\varepsilon}$, C_μ σ_ε and σ_k have the following default values

$C_{1\varepsilon}$ =1.44, $C_{2\varepsilon}$ =1.92, C_μ =0.09, σ_ε =1.3 and σ_k =1.0

These default values have been determined experimentally for fundamental turbulent flows including frequently encountered shear flows like boundary layers, mixing layers and jets as well as for decaying isotropic grid turbulence. They have been found to work fairly well for a wide range of wall-bounded and free shear flows (Ansys Fluent, 2012). But if necessary the constant can be changed.

2.7.3. RENORMALISATION GROUP (RNG) $k-\varepsilon$ MODEL

The RNG $k-\varepsilon$ model is a modified version of the $k-\varepsilon$ model and this provides improved results for swirling flows and flow separation. It is similar in form to the standard $k-\varepsilon$ model, but includes the following refinements: (i) The RNG model has an additional term in its ε equation that improves the accuracy for rapidly strained flows; (ii) The effect of swirl on turbulence is included in the RNG model, enhancing accuracy for swirling flows; (iii) While the standard $k-\varepsilon$ model is a high-Reynolds number model, the RNG theory provides an analytically derived differential formula

for effective viscosity that accounts for low-Reynolds number effects. Effective use of this feature does, however, depend on an appropriate treatment of the near-wall region.

The transport equation for κ is expressed as:

$$\frac{\partial}{\partial t}(\rho\kappa)+\frac{\partial}{\partial x_i}(\rho\kappa\upsilon_i)=\frac{\partial}{\partial x_i}\left[\alpha_k\mu_t\frac{\partial\kappa}{\partial x_i}\right]+G_\kappa+G_b-\rho\varepsilon-Y_M+S_\kappa \qquad (2.32)$$

While the transport equation for ε is expressed as

$$\frac{\partial}{\partial t}(\rho\varepsilon)+\frac{\partial}{\partial x_i}(\rho\varepsilon\upsilon_i)= \frac{\partial}{\partial x_i}\left[\alpha_\varepsilon\mu_t\frac{\partial\varepsilon}{\partial x_i}\right]+C_{1\varepsilon}\frac{\varepsilon}{\kappa}(G_k+C_{3\varepsilon}G_b)-C_{2\varepsilon}\rho\frac{\varepsilon^2}{\kappa}-R_\varepsilon+S_\varepsilon \qquad (2.33)$$

The constants and the values are the same as in the standard $k-\varepsilon$ model with $C_\mu = 0.0845$ at high Reynolds number. At low Reynolds number, the following equation is integrated to obtain μ_t.

$$d\left(\frac{\rho^2\kappa}{\sqrt{\varepsilon\mu}}\right)=1.72\frac{\hat{\nu}}{\sqrt{\hat{\nu}^3-1+C_\nu}}d\hat{\nu} \qquad (2.34)$$

where $C_\nu \approx 100$ and the μ_t is calculated from

$$\mu_t=\hat{\nu}\mu \qquad (2.35)$$

2.7.4. REALIZABLE $k-\varepsilon$ MODEL

The realizable $k-\varepsilon$ model differs from the standard $k-\varepsilon$ model in two ways. (i) The realizable $k-\varepsilon$ model contains an alternative formulation for the turbulent viscosity;

(ii) A modified transport equation for the dissipation rate, ε **,** has been derived from an exact equation for the transport of the mean-square vorticity fluctuation**.**

The transport equation for κ in the realizable $\kappa-\varepsilon$ model is the same to standard $\kappa-\varepsilon$ model. The modified realizable ε model is expressed as:

$$\frac{\partial}{\partial t}(\rho\varepsilon)+\frac{\partial}{\partial x_i}(\rho\varepsilon\upsilon_i)= \frac{\partial}{\partial x_i}\left[\left(\mu+\frac{\mu_t}{\sigma_\varepsilon}\right)\frac{\partial\varepsilon}{\partial x_i}\right]+\rho C_1 S_\varepsilon-\rho C_2\frac{\varepsilon^2}{\kappa+\sqrt{\nu\varepsilon}}+C_{1\varepsilon}\frac{\varepsilon}{\kappa}C_{3\varepsilon}G_b+S_\varepsilon \tag{2.36}$$

where

$$C_1=\max\left[0.43,\frac{\eta}{\eta+5}\right],\eta=S\frac{\kappa}{\varepsilon},S=2S_{i,j}S_{i,j} \tag{2.37}$$

Equation 2.38 is used to calculate turbulent viscosity, μ_t with C_μ as computed as:

$$C_\mu=\frac{1}{A_0+A_s\frac{kU^*}{\varepsilon}} \tag{2.38}$$

The main components of any mixing vessels are the impellers and baffles which helps in homogenization of substances. From the literature reviewed, it was observed that homogeneity is the principal objective of any mixing process. The flow field can be achieved in diverse modelling and simulation processes. The governing equations outlined in this chapter were used in ANSYS FLUENT software to determine the flow field in the next chapter.

CHAPTER THREE

METHODOLOGY

This chapter generally describes the tools and procedures used in obtaining the data that were analyzed in the proceeding chapter. This chapter is divided into two main sections with the first describing the computational domain which described the detailed physical structure of the mixing tank such as the dimensions of the tank, the impeller and its speed and the dimensions of the baffles as well as the computational model or model description. The second part of this chapter also describes the model of impeller rotation, the boundary conditions, the solution model, the flow models, and the dispersed flow model.

3.1. MODEL DESCRIPTION

For any fluid flow problem in ANSYS FLUENT, a domain (a meshed geometry) in which the flow takes place, to evaluate the solution needs to be provided. The geometry used in this present work was a cylindrical flat bottom leaching tank of diameter (T) 12.0 m, height (H) of 12.8 m and volume (V) of 1400 m^3. The tank was equipped with four baffles uniformly spaced at 90 degrees of width T/15.6 around the tank periphery. The tank has a one inlet located at the top and one outlet 12.4 m from the bottom of the tank on the side of the cylinder. Mixing is by mechanical agitation of two hydrofoil impellers. Each impeller has a diameter (D) of T/3 and consists of four blades with pitch angles varying from 45 degrees at the hob at about 22 degrees at the impeller tip. The two impellers are mounted on a shaft concentric with the axis of the vessel with the bottom impeller having off-bottom clearance (L) of H/3.6m. The shaft is driven by a rotational speed of 16 rpm using a motor.

The required geometry of the leaching tank with four baffles at 90° to each other and double impellers were designed using a 3-Dimensional Computer Aided Design (3D CAD) known as Salome 7.7.1 as shown in Figure 3.1. The domain has two zones namely; stationary and moving zones. The moving zone includes the impellers/stirrers and cylindrical disk volume around the impeller while the stationary zone includes the area around the baffles. Both zones are connected by interface.

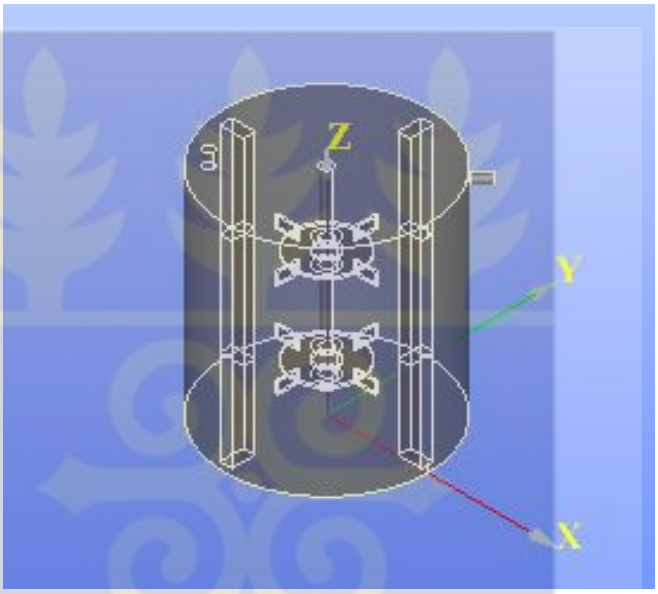

Figure 3.1: A schematic diagram of the geometry

The meshing of the geometry was based on the physics and size of the problem and was carried out using ANSYS meshing in ANSYS workbench. Three different mesh types are available namely; unstructured polyhedral, unstructured tetrahedral and structured hexahedral.

Generally, polyhedral meshes are more computationally efficient than tetrahedral or hexahedral meshes. This is due to the fact that tetrahedral cells have only four faces, whereas the polyhedral cells typically have twelve to fourteen faces. This means that polyhedral cells have a greater number of neighbors and therefore communicate with more cells, allowing the solution to propagate throughout the domain much more rapidly. Also, although polyhedral cells have a greater number of faces, there will

typically be fewer cells in total and therefore fewer faces overall in a polyhedral mesh of a given domain. Thus, polyhedral mesh was used in the simulations presented in this thesis as shown in Figure 3.2. The mesh quality criterial was based on orthogonal quality which ranges from 0 to 1 with values close to zero having lower quality and values close to one having high quality. The minimum orthogonal quality of the mesh used in this work is $4.26935\,e^{-1}$. The mesh contains 526721 cells, 1095213 faces and 109436 nodes.

Figure 3.2: Meshed geometry

3.2. MODEL DESCRIPTION

Leaching processes between solid and liquid normally occurs in turbulent regime. Therefore, in this thesis, multiphase flow as well as turbulent models have been adopted for the computational simulations.

3.2.1. Conservation Equation of Multiphase Flow

The Eulerian-Eulerian multi-fluid model with enhanced wall function was used in this simulation. The liquid and solid phases were all treated as different continua, interpenetrating and relating with each other everywhere in the computational domain. The continuity and momentum govern their particular phases. The pressure field is supposed to be shared by all the phases according to their volume fraction.

Since the leaching process does not involve heat transfer, only the continuity and momentum equations are solved based on the Eulerian-Eulerian model. Details of this model has been presented in Section 2.6 of Chapter two. The governing equations for the continuity and momentum have been modelled as presented below.

Continuity equation:

$$\frac{\partial(\alpha_q \rho_q)}{\partial t} + \nabla.(\alpha_q \rho_q U_{q,i}) = 0, \tag{3.1}$$

Momentum equation:

$$\begin{aligned} &\frac{\partial}{\partial t}(\alpha_q \rho_q U_{q,i}) + \nabla.(\alpha_q \rho_q U_{q,i} U_{q,i}) = \\ &-\alpha_q \nabla p - \nabla\left(\alpha_q \overset{=(lam)}{\tau}_{q,ij}\right) - \nabla.\left(\alpha_q \overset{=(t)}{\tau}_{q,ij}\right) + \alpha_q \rho_q g_i + F_{td} + F_M \end{aligned} \tag{3.2}$$

where q denotes the phase of the material and *i* is the direction. U_q and α_q are the time-averaged values of the velocity and volume fraction of phase q respectively. P is the time-averaged pressure. ρ_q is the density of the phase. $\alpha_q \rho_q g_i$ is the external body force on the phase q. F_{td} is the turbulent dispersion force accounting for the fluctuations in the phase volume fraction. F_M is the time-averaged inter-phase force in i direction. $\overset{=(lam)}{\tau}_{q,ij}$ is the stress tensor in phase q due to viscosity. $\overset{=(t)}{\tau}_{q,ij}$ is the Reynolds stress, representing the effect of turbulent fluctuations on the convective transport over the averaging time period. In the conservation equations, the forces that need to be modelled are the Reynolds stress, turbulent dispersion and the inter-phase force.

3.2.1.1 Effects of Turbulent Fluctuations of The Liquid Phase

To account for the effects of turbulent fluctuations of the liquid phase, the turbulent dispersion force (a term in the momentum equation (3.2)) was modelled. For dispersed flows, the turbulent dispersion force acts as a turbulent diffusion and its contribution is significant when the size of eddies becomes larger than the particle size (Angst *et al.*, 2001; Lopez de Bertodano, 1992) highlights the importance of modelling turbulent dispersion force while simulating solid suspension in stirred reactors. Thus, in this thesis, the turbulent dispersion force was modelled using the equation (Lopez de Bertodano, 1992).

$$F_{td} = C_{td}\rho_1 k_1 \nabla \varepsilon_1 \qquad (3.3)$$

Where F_{td} is the turbulent dispersion force, ρ_1 is the continuous phase density, k_1 is the turbulent kinetic energy in the continuous phase, ε_1 is the gradient of the dispersed phase and C_{td} is the turbulent dispersion coefficient, C_{td} is in the range of 0.1 – 1.0. A C_{td} value of 0.1 was used in this work.

3.2.1.2 Interphase Momentum Transfer

Interphase momentum transfer occurs due to interfacial forces acting on each phase, owing to interaction with another. The various mechanisms that comprise drag, lift and added mass forces involve the interaction of the phases. However, only the contribution of drag force has been considered in this study because the other forces have no effect on solid-liquid hydrodynamics in stirred tanks (Khorkpor et al., 2004). The drag force exerted by the dispersed phase on the continuous phase was modelled as:

$$F_{12,i} = \frac{3\alpha_1\alpha_2\rho_1 C_D\left[\sum\left(U_{2,i}-U_{1,i}\right)^2\right]^{0.5}\left(U_{2,i}-U_{1,i}\right)}{4d_p}, \qquad (3.4)$$

where C_D is the drag coefficient, exerted by the liquid phase on the solid phase and $4d_p$ is the solid particle diameter. The drag coefficient was obtained by the turbulence correction factor expressed as:

$$\frac{C_D - C_{D0}}{C_{D0}} = 8.76\times10^{-5}\left(\frac{d_p}{\lambda}\right)^3 \qquad (3.5)$$

where λ is the Kolmogorov length scale, d_p is the mean particle diameter and C_{D0} is the drag coefficient in a stagnant liquid calculated as follows:

$$C_{D0} = \frac{24}{\mathrm{Re}_p}\times\left(1+0.15\mathrm{Re}_p^{0.687}\right) \qquad (3.6)$$

where Re_p is the Reynolds number of the particle.

3.2.2. Modelling Turbulence

Turbulence modelling is the construction and use of a model to predict the effects of turbulence. Three turbulent models (standard $k-\varepsilon$ model, the RNG $k-\varepsilon$ model and the realizable $k-\varepsilon$ model) have been simulated in this thesis and the results have been compared to obtain the best turbulent model. The details of the governing transport equations for all the three turbulent models have been presented in Chapter 2 Section 2.8.

3.2.3. Modelling Of Impeller Rotation

As noted, the flow domain consists of two zones: stationary (the tank, baffles and the flow outside the impeller frame) and moving zones (the impeller). To model the

impeller rotation, the Multiple Reference Frame (MRF) model was used. The MRF model is a steady-state approximation in which individual cell zones are assigned different rotational and/or translational speeds. The flow in each moving cell zone was solved using the moving reference frame equations as presented in Chapter 2 Section 2.7.

3.2. BOUNDARY CONDITIONS

The cell zone consists of state of the material in the respective zones. The mixture of sand-liquid solution or slurry was considered a multiphase mixture. Thus, to obtain a well-posed system of equations, reasonable boundary conditions for the computational domain were implemented. Velocity inlet boundary condition was specified for both the liquid and sand respectively. Pressure outlet boundary conditions were used to define the static pressure at flow outlet. The rotation of the impeller in the fluid domain was defined as moving reference frame with rotational speed of 16rpm about the z-axis. Stationary options were enabled in the rest of the fluid domain. No-slip boundary condition with standard wall functions was enforced at tank walls, impeller surfaces and baffles defined with stationary wall motion. The fluid surface of the tank was modeled as slip wall with zero shear (i.e. wall is frictionless and exert no shear stress on the adjacent fluid).

3.3. SOLUTION METHOD

The simulation was performed using ANSYS FLUENT 14.5 solver in which all the models for multiphase, RTD and turbulence calculations are fixed in the solver. FLUENT uses control-volume-based technique to convert a general scalar transport equation to an algebraic equation that can be solved numerically using either the density-based solver or the pressure-based solver. In this technique, the transport

equations are integrated on the individual control volumes, in the flow domain, to construct algebraic equations for the discrete dependent variables (unknowns) such as velocities, pressure, and temperature and conserved scalars. The density based approach is mainly used for high-speed compressible flows while the pressure-based solver is used for low speed incompressible flows. In a leaching tank, low speed agitation is employed during mixing in order to prevent carbon degradation. Thus, in this study the pressure-based solver with segregated algorithm was used to solve the governing equations by iterations in which the entire set of nonlinear and coupled equations was solved repeatedly until the solution converges. The pressure equation was derived from continuity and momentum equation in such a way that the velocity field, corrected by the pressure, satisfies the continuity equation.

In the segregated algorithm, the individual governing equations for the solution variables are solved one after another. While being solved, each governing equation is decoupled or segregated from other equations. The segregated algorithm is memory-efficient, since the discretized equations need only be stored in the memory one at a time. Inasmuch as the equations are solved in a decoupled manner, the solution convergence is relatively slow. The phase coupled Semi-Implicit Method for Pressure-Linked Equations (PC-SIMPLE) algorithm for the pressure-velocity coupling is an extension of the SIMPLE algorithm to multiphase flows. The pressure-velocity coupling refers to the numerical algorithm which uses a combination of continuity and momentum equations to derive an equation for pressure or pressure correction when using the pressure-based solver. Four algorithms are available in FLUENT but the default scheme SIMPLE algorithm which is recommended for turbulent multiphase flows to obtain quick solution convergence was used. The SIMPLE algorithm uses the relationship between velocity and pressure corrections to enforce mass conservation

and to obtain the pressure field. The velocities are solved coupled by phases, but in a segregated fashion. The gradient of the spatial discretization was set to least square cell based momentum of second order upwind. The volume fraction was set to First Order Upwind with Second Order Upwind specified for the turbulent kinetic Energy and the turbulent Dissipation Rate.

The solution was initialized from the inlet. Convergence was achieved when the residuals on continuity, velocities, turbulent kinetic energy and turbulent dissipation rate fell below $10e^{-5}$ and became constant. The convergence criterial are preset conditions for the residuals that determine when an iterative solution is converged. The assumption for any set of convergence criterial is that the solution is no longer changing with more iteration and when the condition is reached, there is an overall mass balance throughout the domain.

In conclusion, the governing equations discussed in the preceding chapter were applied through the ANSYS FLUENT software as a Computational Fluid Dynamics (CFD) tool for the modelling of the reactor vessel and the simulation of the mixing process in this Chapter. The procedures outlined in this chapter aided in determining some velocity flow vectors, velocity contour plots, sand and water volume fractions and eddy viscosity of the flow field. The results of these flow characteristics have been analyzed in the proceeding chapter.

CHAPTER FOUR

RESULTS AND DISCUSSION

Analysis of the data obtained from the use of ANSYS FLUENT software as a Computational Fluid Dynamics (CFD) tool is presented in this Chapter. Where the results of the turbulence model on mixing is presented.

Under the Section which discusses the effects of turbulence model on mixing, the flow field and the flow distribution of the sand and water materials are presented. Three different $k-\varepsilon$ turbulence models have been used and the results are compared. In the analysis of the flow field, the sand and water velocity vector plots have been discussed in relation to the turbulence models. In addition, the contour profiles of the flow distribution which encompassed the sand and water velocities, sand and water axial velocities, sand and water radial velocities and the sand and water volume fractions in the tank domain have been discussed. The first part of this Chapter ended with the discussions of the eddy viscosity and the turbulent kinetic energy of the material.

4.1 EFFECTS OF TURBULENCE MODEL ON MIXING

4.1.1 Flow Field

4.1.1.1 Sand and Water Vector Plots

In Figures 4.1a and 4.1b, the velocity vector plot of both the sand and water using the realizable $k-\varepsilon$ model are respectively shown. The velocity vector profile depicts an evenly zero velocity vector for both sand and water in the tank domain. The outlet of the tank shows a relatively high velocity compared to the domain. The zero velocity in the domain could be due to the fact that the Realizable $k-\varepsilon$ model cannot account for

domains with both rotating and stationary fluid zones as is the case of the model configuration used in this thesis.

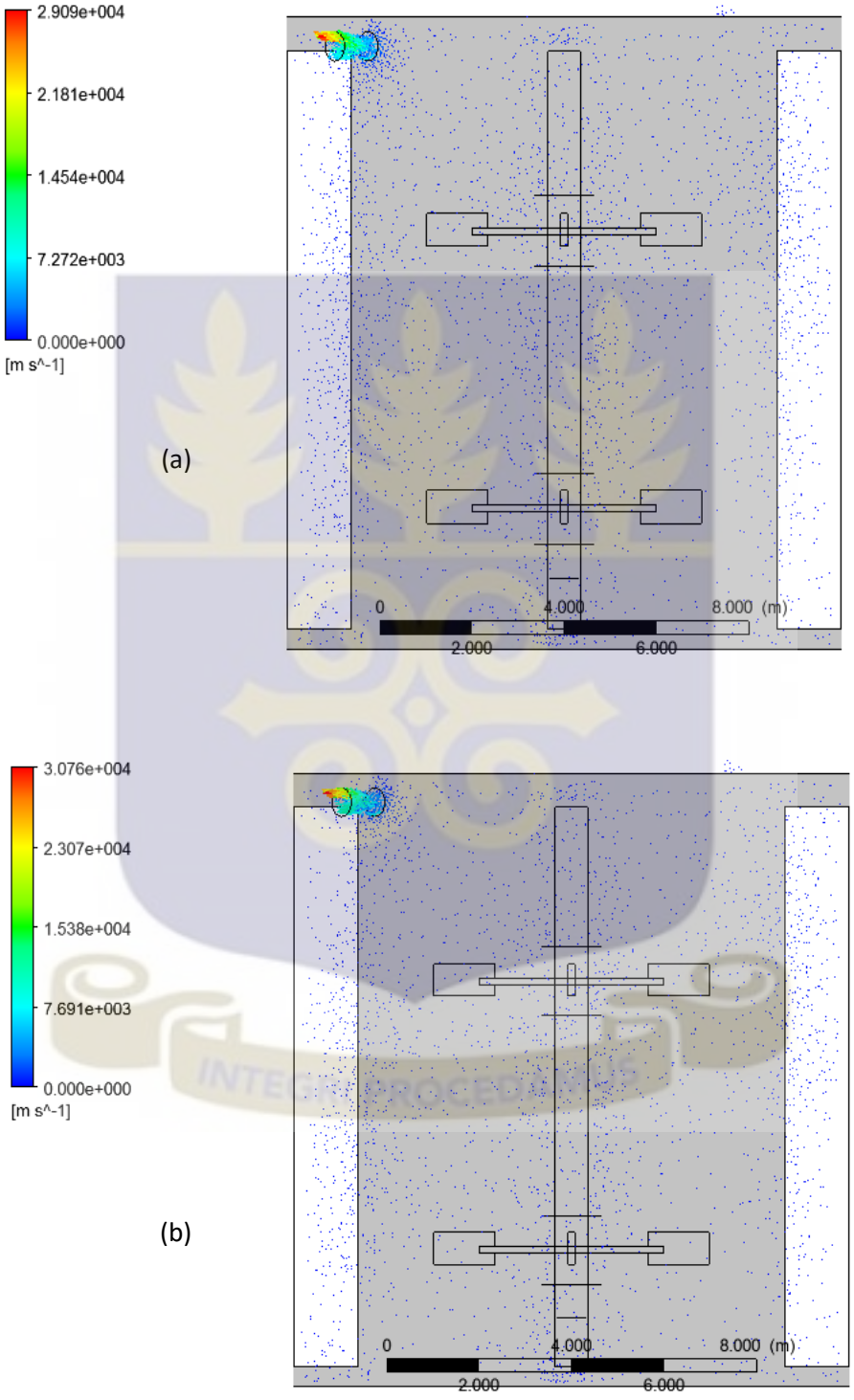

Figure 4.1: Velocity vector plot for Realizable $k-\varepsilon$ model; (a) Sand (b) water

Using the RNG $k-\varepsilon$ model to analyse the flow field in the tank, Figure 4.2a depicts the flow field of the sand material. The sand velocity vector is generally low, however, this low velocity vector is largely concentrated around the region of the shaft and less concentrated in the regions of the baffles in the tank domain.

Contrary to the velocity profile in Figure 4.2a, the vector plot of the water velocity profile as shown in Figure 4.2b depicts a higher velocity vector than that of the sand. The water velocity vector is largely concentrated in the regions between the lower and upper impeller shaft and less concentrated in the regions of the baffles and the tank domain.

The RNG $k-\varepsilon$ model is limited to only flows containing swirls or vortex thereby accounting for the result obtained from Figure 4.2.

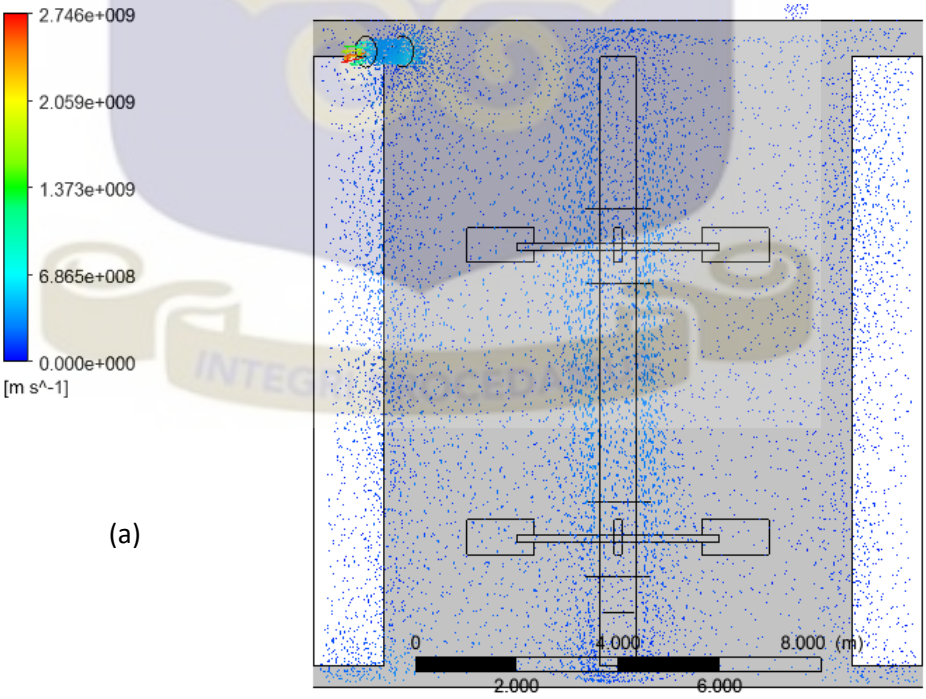

(a)

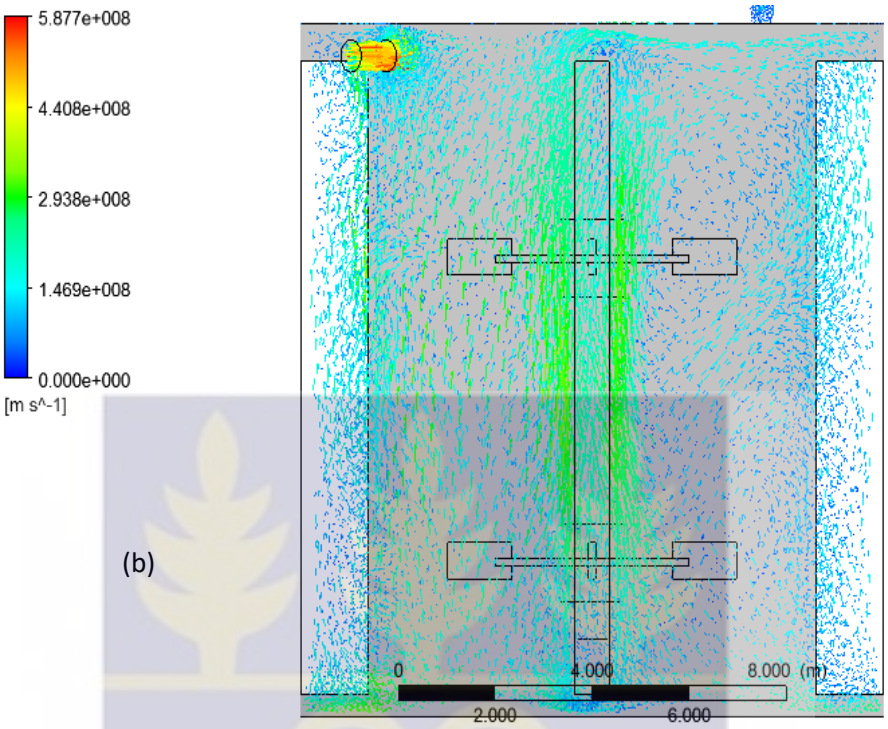

Figure 4.2:Velocity vector for RNG $k-\varepsilon$ model; (a) Sand (b) Water

In Figure 4.3, the velocity vector plot for both sand and water using the Standard $k-\varepsilon$ model is presented. The instabilities in the flow field exhibits symmetrical axial flow outline. It is observed that the distribution of the velocity fields differ significantly in the flow domain where the highest velocity magnitude is observed along the baffles and the impeller shaft. The liquid injected at the inlet from the top of the tank moves downwards in the axial direction along the right baffles and moves tangentially towards the bottom of the tank. A portion of the stream moving upwards forms a circular movement while the remaining stream continue the upward movement along the left baffle and then returns downward to rejoin the flow.

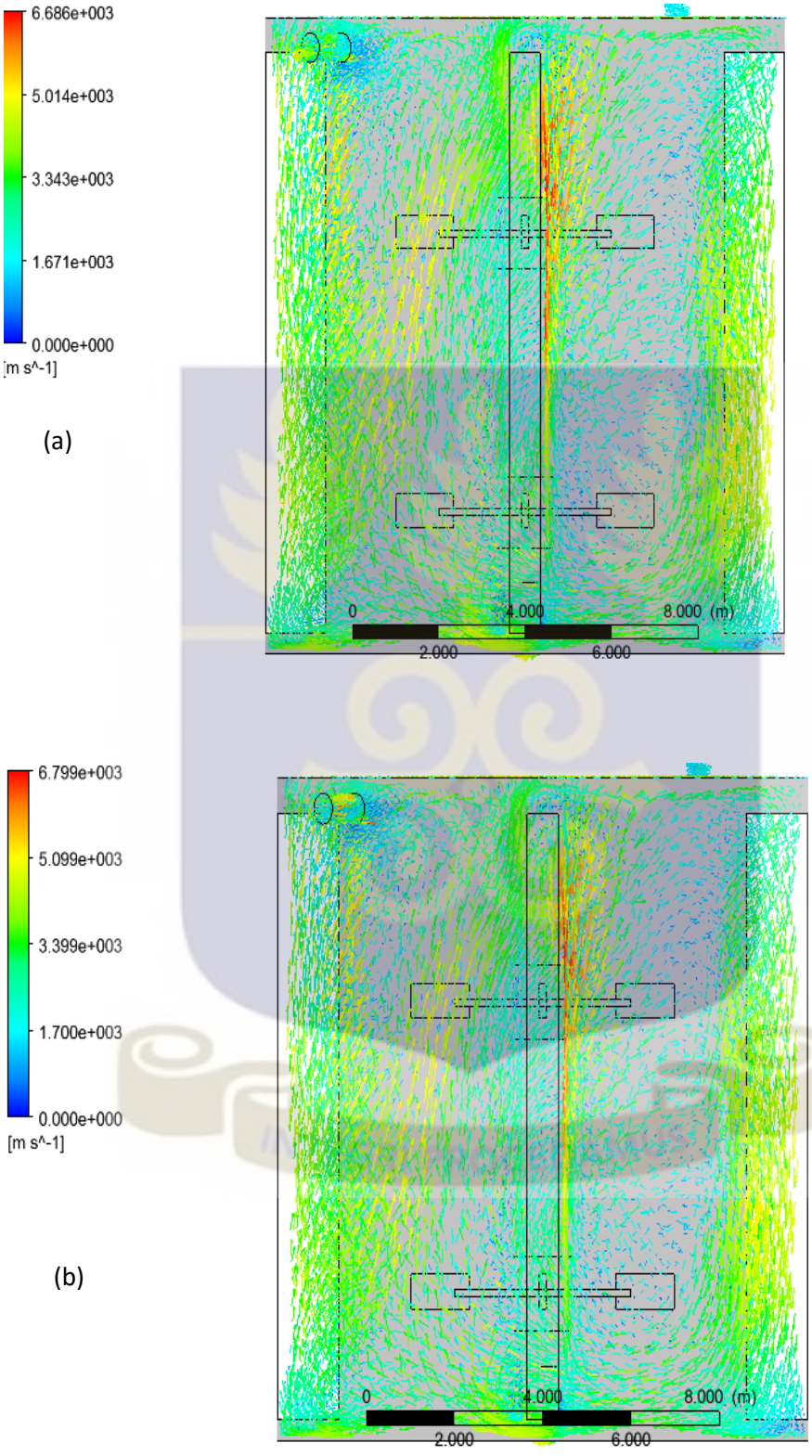

Figure 4.3: Velocity vector for Standard $k-\varepsilon$ model; (a) Sand (b) Water

It is observed that the liquid movement culminated in circular loops (vortex) formation where two kinds of circulation loops can be observed. These consists of two turbulent major loops around the two baffles and the impeller shaft. Also, there is a minor loop around the lower right impeller. It is observed that the loops are more evident in the discharge region of the baffle and shaft. This can be explained by the long length of the impellers compared to the diameter of the tank.

This makes the space between the impellers and the baffles smaller, so the liquid when stirred by the impellers are taken up by the baffles or tank walls. Similarly, the size of the shaft which is broad hinders part of the flow in the tank domain thereby resulting in a strong circulation loop around the baffles and the shaft.

In the flow fields described above in the Figures 4.1, 4.2 and 4.3 it can be deduced that the standard $k-\varepsilon$ model gives the best flow field amongst the three models. This is because, even though the RNG and the Realizable $k-\varepsilon$ model are the modification on the standard $k-\varepsilon$ model, they have limitations. The modification of RNG $k-\varepsilon$ model is in the areas of strain and swirl flow, whereas the realizable $k-\varepsilon$ model is limited in the areas where both rotating and stationary fluid zones exist.

4.1.2 Flow Distribution

4.1.2.1 Sand and Water Velocity Magnitude

In Figure 4.4 the velocity magnitude of sand and water using the realizable $k-\varepsilon$ model are presented.

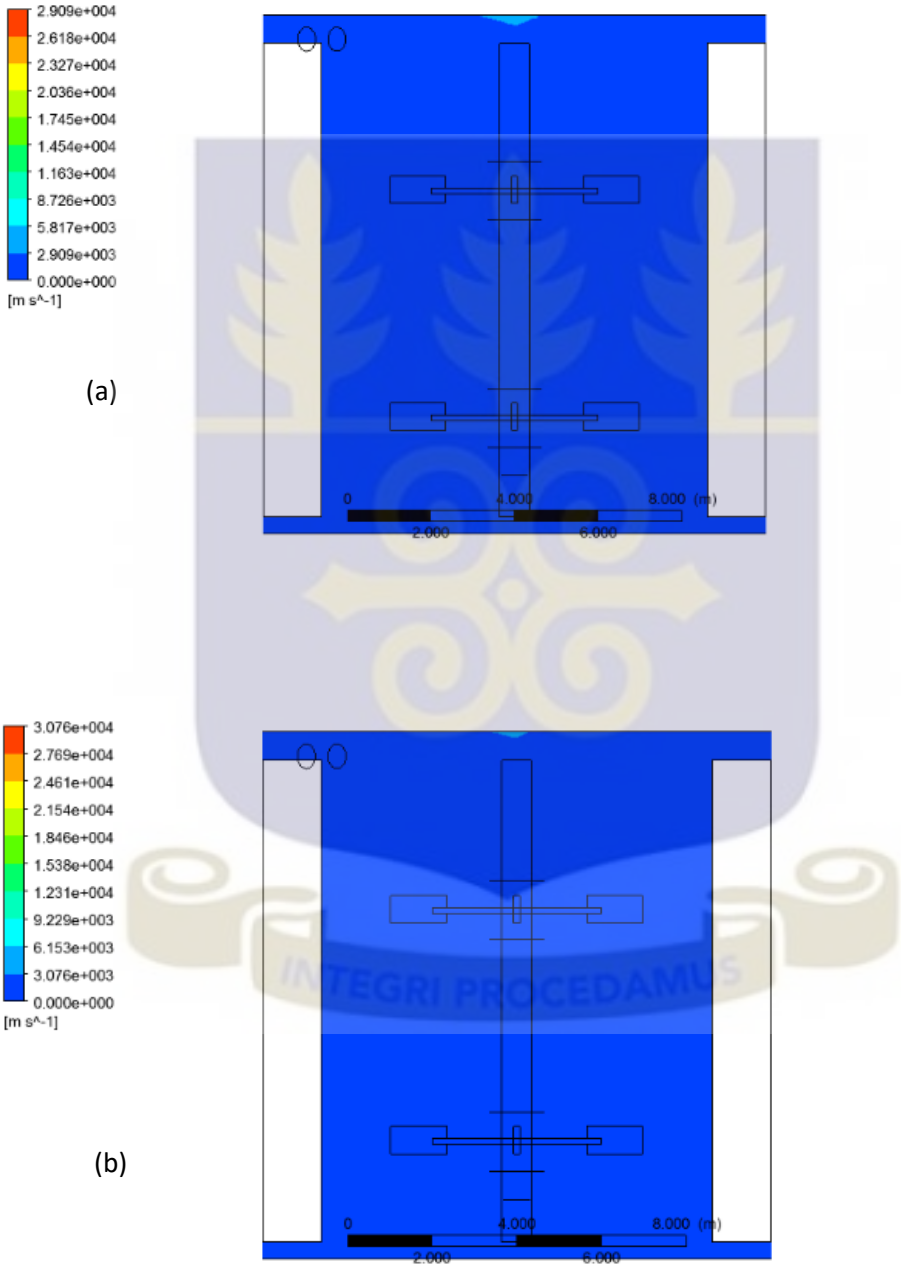

Figure 4.4: Contour plots of Velocity magnitude for Realizable $k-\varepsilon$ model; (a) Sand, (b) Water

From Figure 4.4, it is observed that the sand and water velocity in the entire tank domain is very low, almost zero similar to the velocity vector plots shown in Figure 4.1.

Using the RNG $k-\varepsilon$ model, as shown in Figure 4.5, it can be observed that the sand velocity magnitude is very low similar to the trend observed in Figure 4.4. However, unlike Figure 4.4 where both the sand and the water velocity magnitude depicted an almost zero velocity, Figure 4.5b which show some variations in the velocity magnitude. From Figure 4.5b, it is observed that the water velocity around the central portion of the tank near the left side of the baffle is very low.

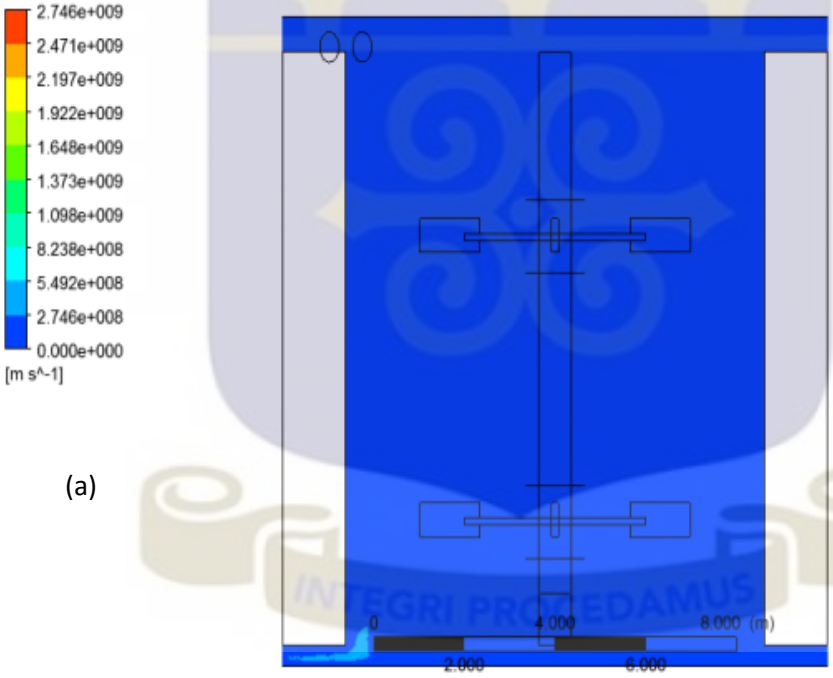

(a)

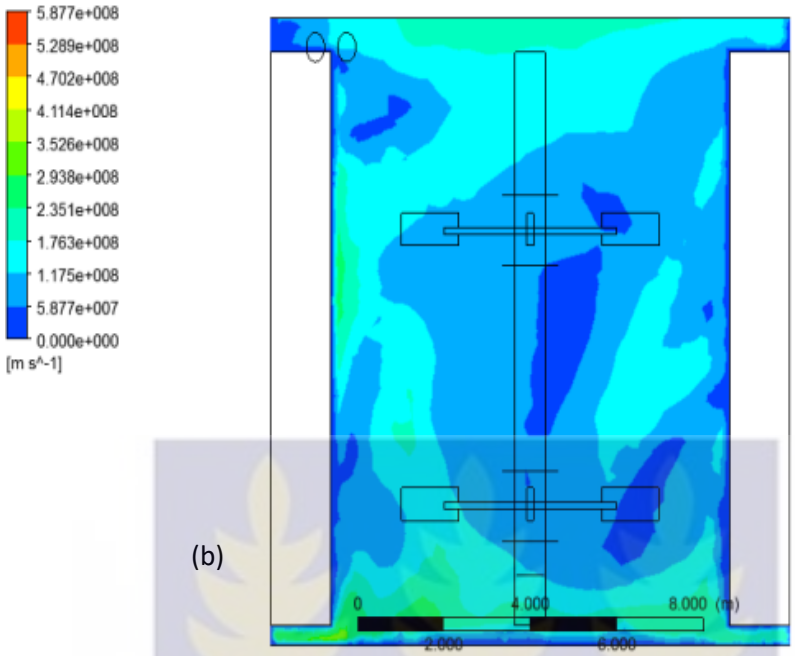

Figure 4.5: Velocity for RNG $k-\varepsilon$ model; (a) Sand, (b) Water

However, the bottom portion of the tank and the portion around the impeller to the top of the tank shows a better water velocity magnitude than the central portion. The velocity contour plot can also be related to the RNG $k-\varepsilon$ model showing similar trend in the water velocity vector plot and none in the sand velocity vector plot.

Figures 4.6a and 4.6b show the sand and water velocity contour plot in the tank using the standard $k-\varepsilon$ model. It is observed that the distribution of sand and water velocities differ significantly in the flow domain where the highest velocity magnitude of the material (sand and water) is observed around the baffle tips.

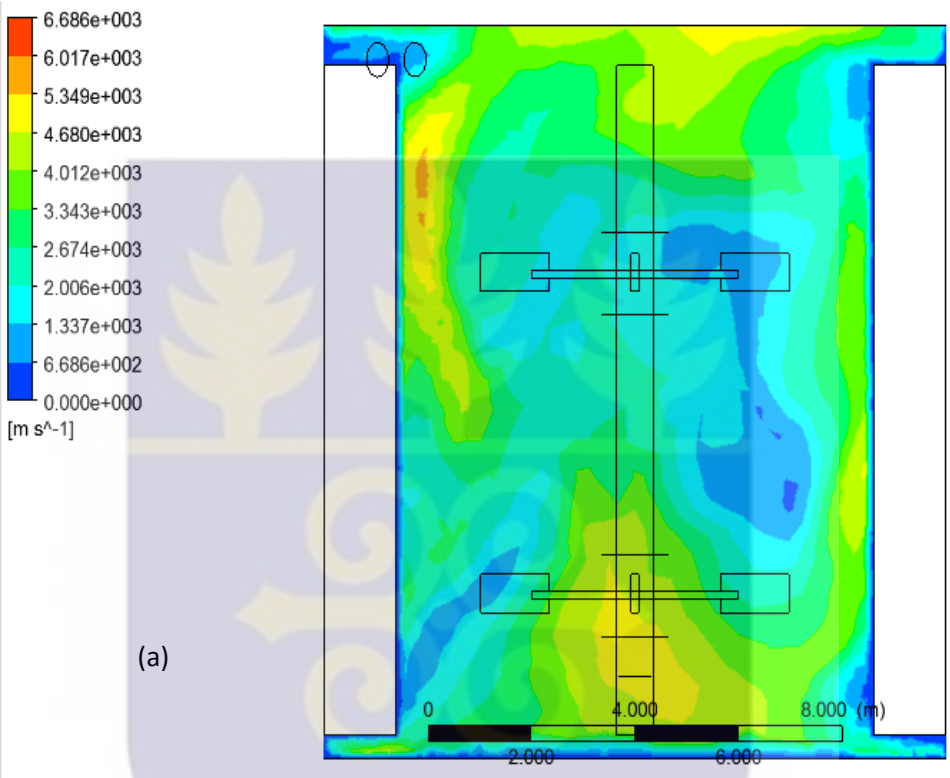

(a)

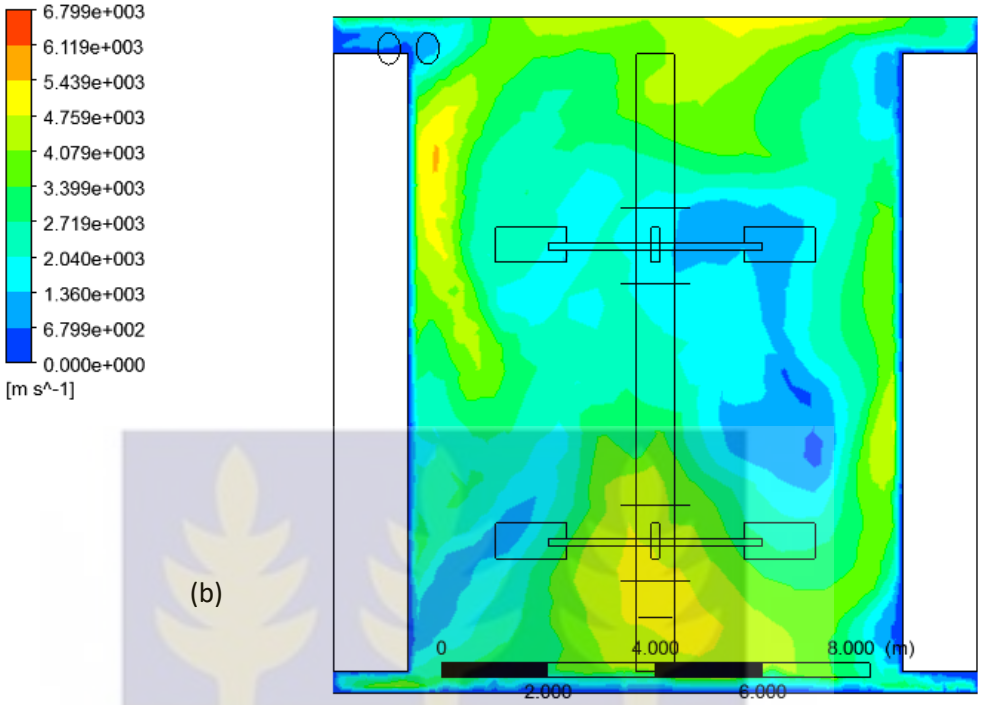

Figure 4.6:Velocity for Standard $k-\varepsilon$ model; (a) Sand, (b) Water

Furthermore, the central portion at the bottom of the tank and the topmost part of the tank also has high sand and water velocities. Also, the areas around the impellers and the central portion of the shaft indicates less sand and water velocity magnitudes in the tank domain. This indicates uneven distribution of velocity in the domain of the tank. The high velocities recorded for both sand and water in the domain shows there is good off bottom suspension in the tank. This means that the sand would not be settled in the bottom of the tank which is good attribute for mixing.

In a turbulent regime, a higher velocity of the bulk fluid will result in effective mixing of the materials (sand and water). Therefore, comparing the profiles of contour plots of velocity magnitude for both sand and water using the three $k-\varepsilon$ turbulence models, it can be observed that the standard $k-\varepsilon$ model depicts the highest sand and water

velocity profiles especially in the regions around the walls of the baffles and the bottom part of the shaft. The high velocity at the bottom of the tank depicts a good off-bottom suspension of the sand particles. The strong tangential velocity component keeps the solids suspended off the tank bottom and will not accumulate over time. This can also be linked to the velocity vectors for both water and sand for standard $k-\varepsilon$ model. The trend in both the water and the sand velocity magnitude and velocity vectors are almost the same.

4.1.2.2 Axial Velocity of Sand and Water

Figure 4.7a represents the upward direction of flow of the sand velocity in the tank domain. From the diagram, the portion of the sand velocity from the bottom of the tank along the left side of the tank near the impeller and baffles represents high sand velocity magnitude.

Also, the other portion around the right side of the tank between the impellers and the baffle represents a low sand velocity in the axial direction.

The axial water velocity in Figure 4.7b generally represents an even velocity in the tank domain with the exception of a small differential axial velocity along the top right portion of the baffle. From the contour plot, the colour contour signifies a low sand velocity in the axial direction.

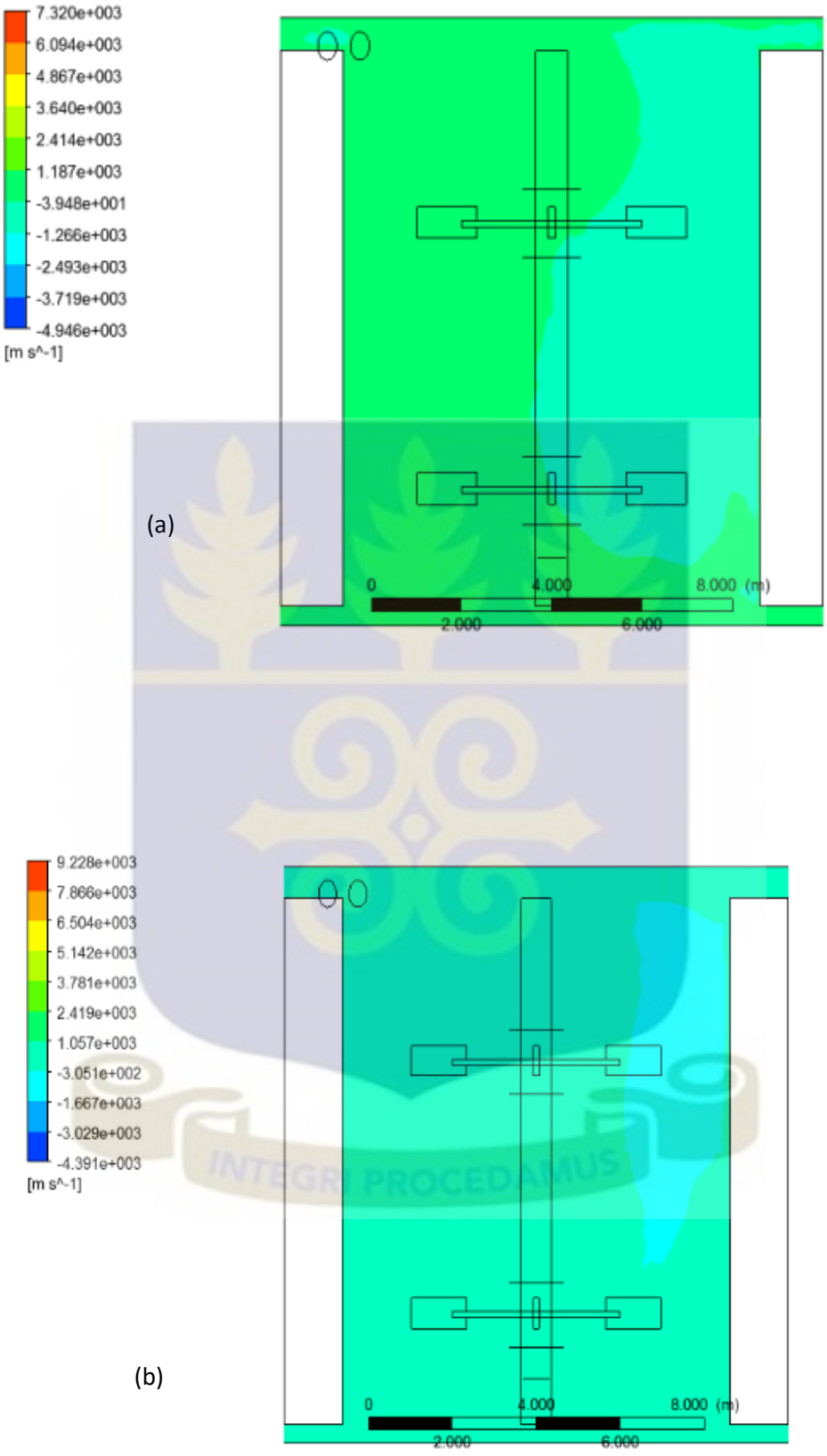

Figure 4.7:Axial velocity for Realizable $k-\varepsilon$ model; (a) Sand, (b) Water

The generally uniform axial velocity output is evident in the uniform colour in the contour profile above. The axial water velocity in Figure 4.7b shows an even distribution contrary to the axial sand velocity in Figure 4.7a. Hitherto, both sand and water axial velocities were analysed using the realizable $k-\varepsilon$ model.

The axial velocity for RNG $k-\varepsilon$ model shown in Figure 4.8 represents the vertical contour plot of the x-z plane of sand and water velocity in the axial direction with enhanced wall function.

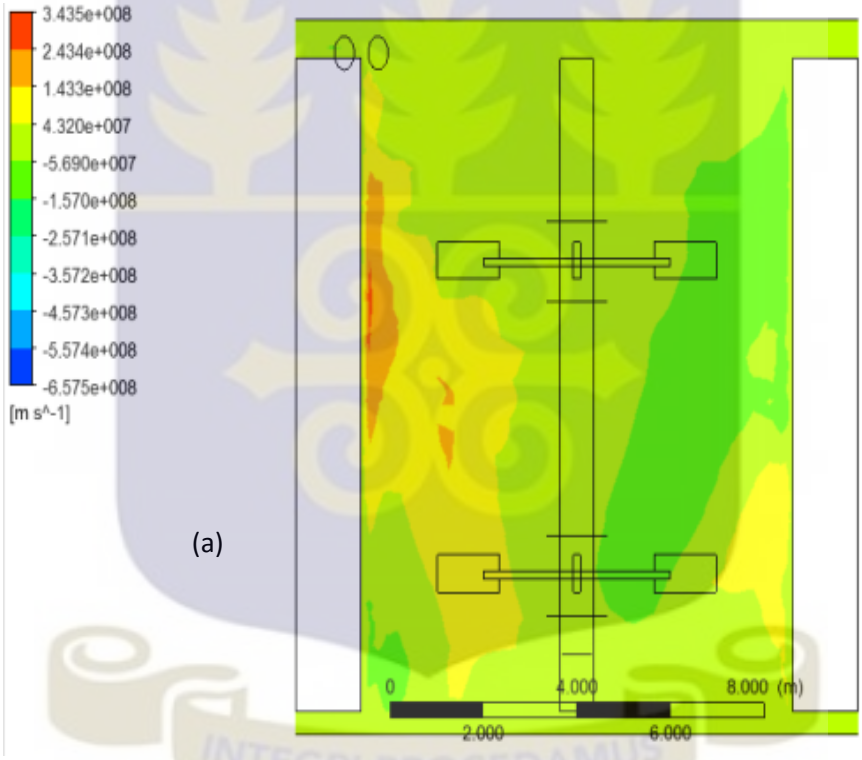

(a)

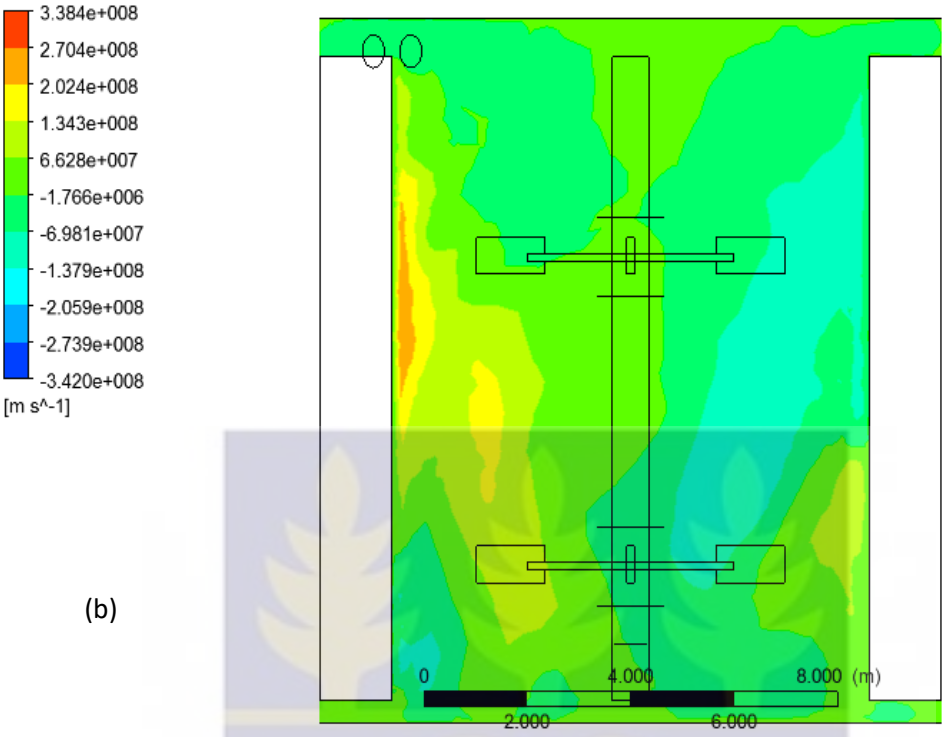

Figure 4.8:Axial velocity for RNG $k-\varepsilon$ model; (a) Sand (b) Water

The sand velocity in the axial direction in the tank generally is very high with the area around the left baffle showing the highest. The central portion to the top of the tank also exhibits a moderately high sand velocity. Also, the top right side of the tank along the baffle is low but the portion down the baffle is high.

The colour contour profile of the axial water velocity is shown in the Figure 4.8b above using the same RNG $k-\varepsilon$ model. The left side of the baffle towards the left bottom exhibits higher axial velocity, as well as the central top and the right bottom of the baffle. Also, the top right of the baffle towards the central portion of the tank displays a relatively low axial water velocity.

Figures 4.9a and 4.9b represent axial velocity for both sand and water respectively using the standard $k-\varepsilon$ model. Both colour contours above generally have high sand

and water velocities in the axial direction with the portion around the top side of the baffle being the highest and the right side along the baffle also being the lowest.

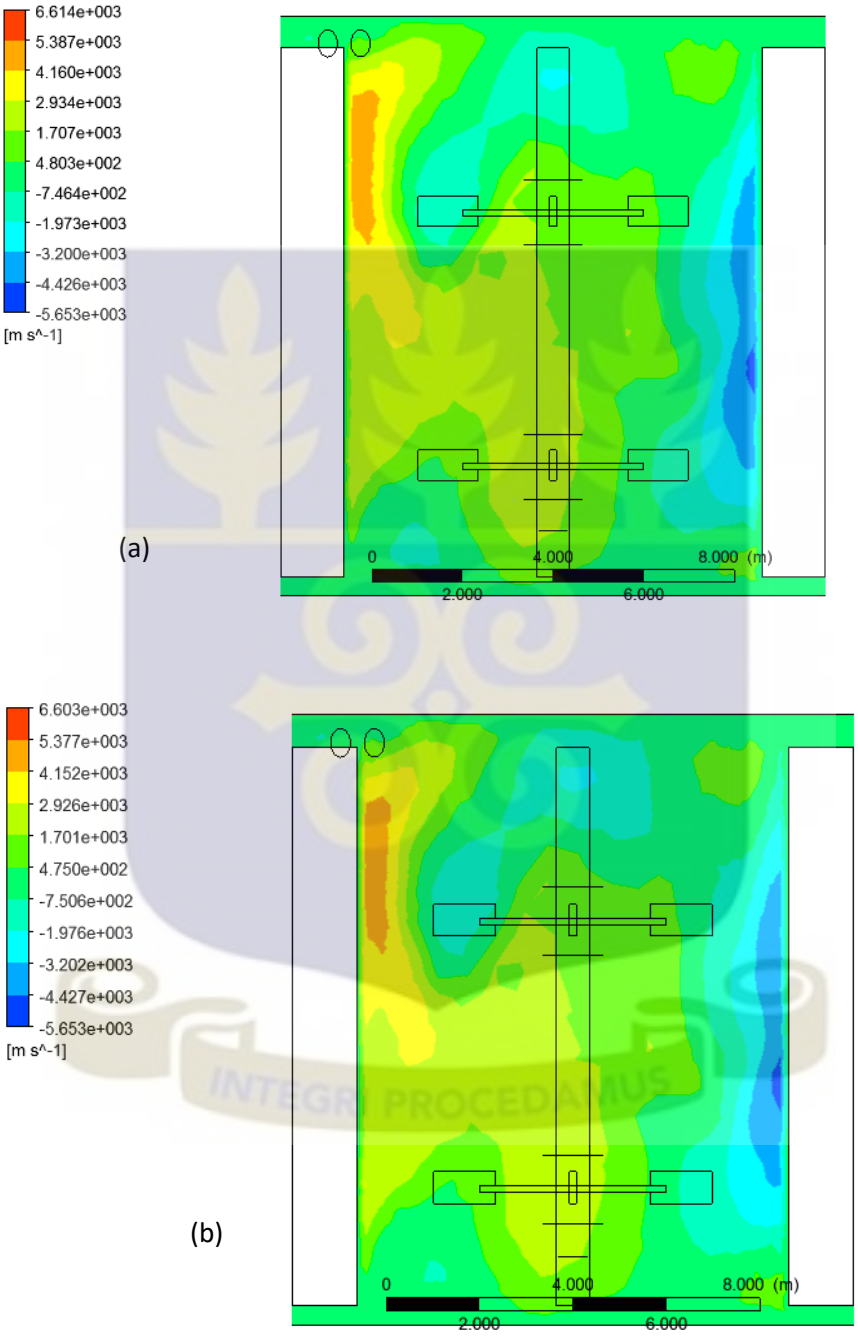

Figure 4.9: Axial velocity for Standard $k-\varepsilon$ model; (a) Sand, (b) Water

Hitherto, the central portion of the tank shows that the axial sand velocity is generally high. The uneven axial sand velocity is evident on the colour contour profile by the different shades of colour in the portions around the top side of the baffle and the right side of the baffle. The above analysis was done using the standard model.

The RNG $k-\varepsilon$ model of the sand and water axial velocities exhibits a much more uniform axial velocity in the tank domain than the sand and water axial velocities using the standard and the realizable $k-\varepsilon$ models. Comparing the velocity vector plots to the axial velocity contour plot, the realizable $k-\varepsilon$ model in both plots gave poor contours. Also, comparing the velocity vector plots to the axial velocity contour plots of both the RNG and the Standard $k-\varepsilon$ model, shows a good relationship in both plots. A relatively high velocity for both sand and water is required for effective mixing to take place.

4.1.2.3 Radial Velocity of Sand and Water

Using the realizable $k-\varepsilon$ model to analyse the sand and water radial velocities in the tank, the colour contours of Figures 4.10a and 4.10b were obtained.

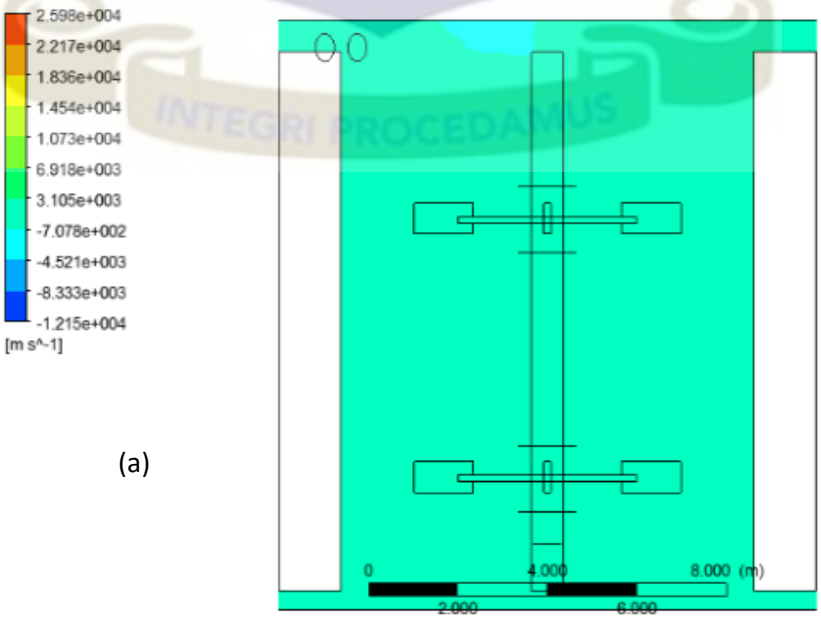

(a)

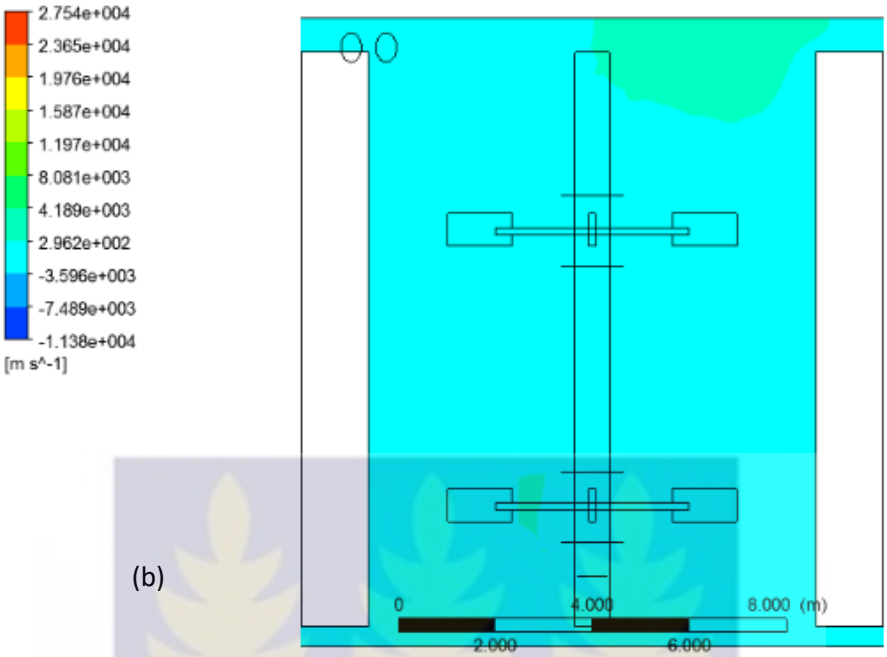

Figure 4.10: Radia velocity for Realizable $k-\varepsilon$ model; (a) Sand (b) Water

Both sand and water profiles generally represent a low uniform velocity in the tank domain. However, the sand profile in Figure 4.10a signifies a higher sand velocity in the radial direction while the water profile in Figure 4.10b signifies a relatively lower radial water velocity.

The Figure 4.11 represents the radial velocity profile using RNG $k-\varepsilon$ model. Figure 4.11a represents a generally high sand velocity in the radial direction but not homogeneous. The top right corner and the bottom left corner of the tank domain from the contour plot represents higher velocity compared to the top left corner and the bottom right corner of the tank domain.

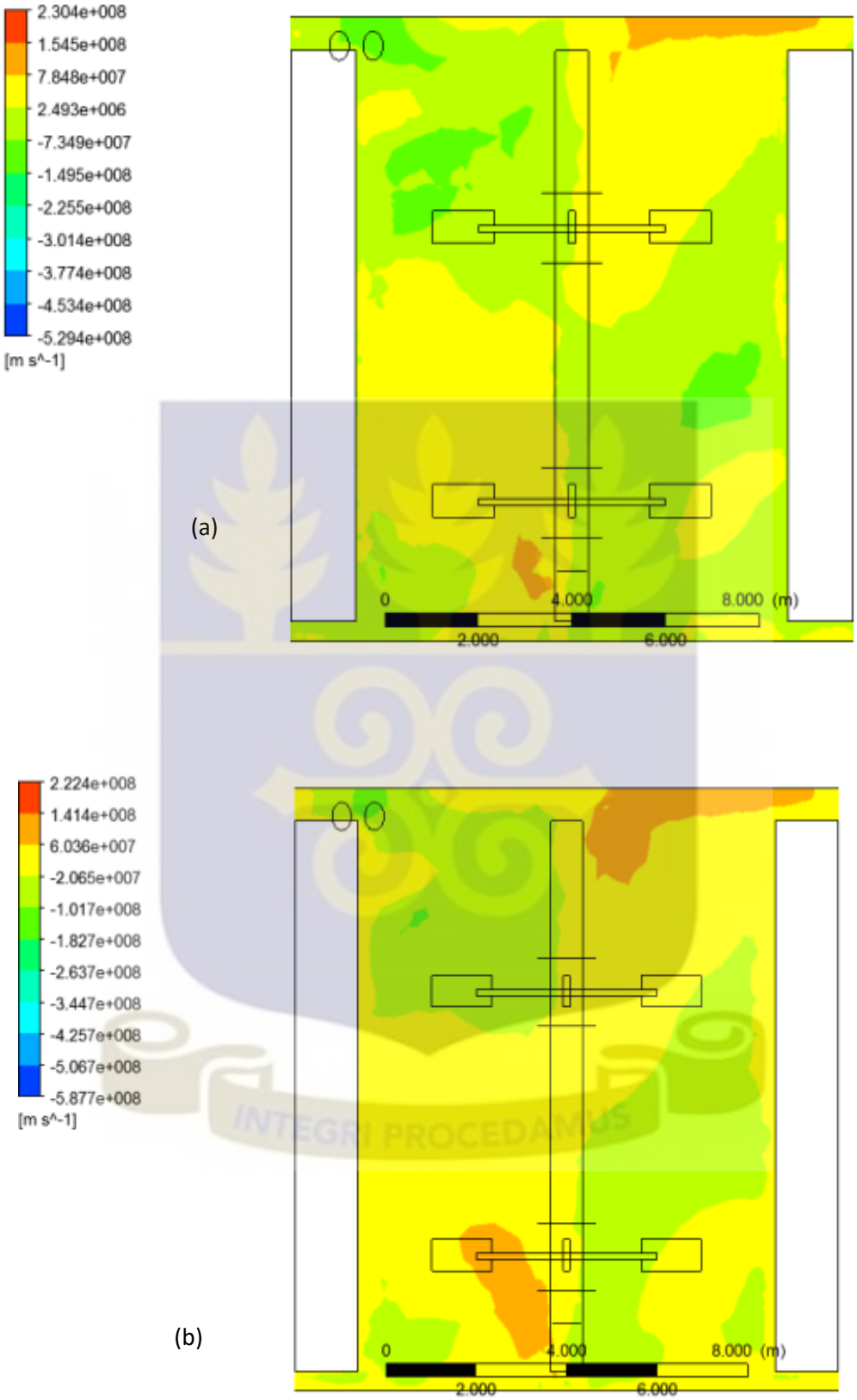

Figure 4.11:Radial velocity for RNG $k-\varepsilon$ model; (a) Sand, (b) Water

Also Figure 4.11b represents the contour plot of water radial velocity of a stirred tank. The colour contour profile depicts a generally high water velocity in the radial direction, except the areas around the top left, the lower part of the shaft towards the upper part of the right baffle. Furthermore, the top right part of the tank and the lower left of the impeller displays relatively higher water velocity radial. Both Figures exhibit inhomogeneous sand and water radial velocities.

The Figure 4.12a represents radial sand velocity using the standard $k-\varepsilon$ model. From the contour plot, it can be observed that, the radial sand velocity is high at the top right corner of the tank diagonally to the bottom left of the tank. Also, the radial sand velocity is relatively low at the top left corner and the bottom right corner of the tank. The relatively uneven radial sand velocity distribution can be seen in the contour colour profile by the different patches of colour in the contour profile.

Similarly, using the standard $k-\varepsilon$ model in analysing the axial water velocity in the tank, the colour contour profile in Figure 4.12b was obtained. The uneven distribution of the axial water velocity is depicted in the contour colour profile by the different colour patches in the Figure 4.12b above. In the portions of the bottom left of the tank and the upper portion of the shaft, the profile shows relatively high axial water velocity. Hitherto, portions around the lower right of the tank around the right baffle shows a lower axial water velocity.

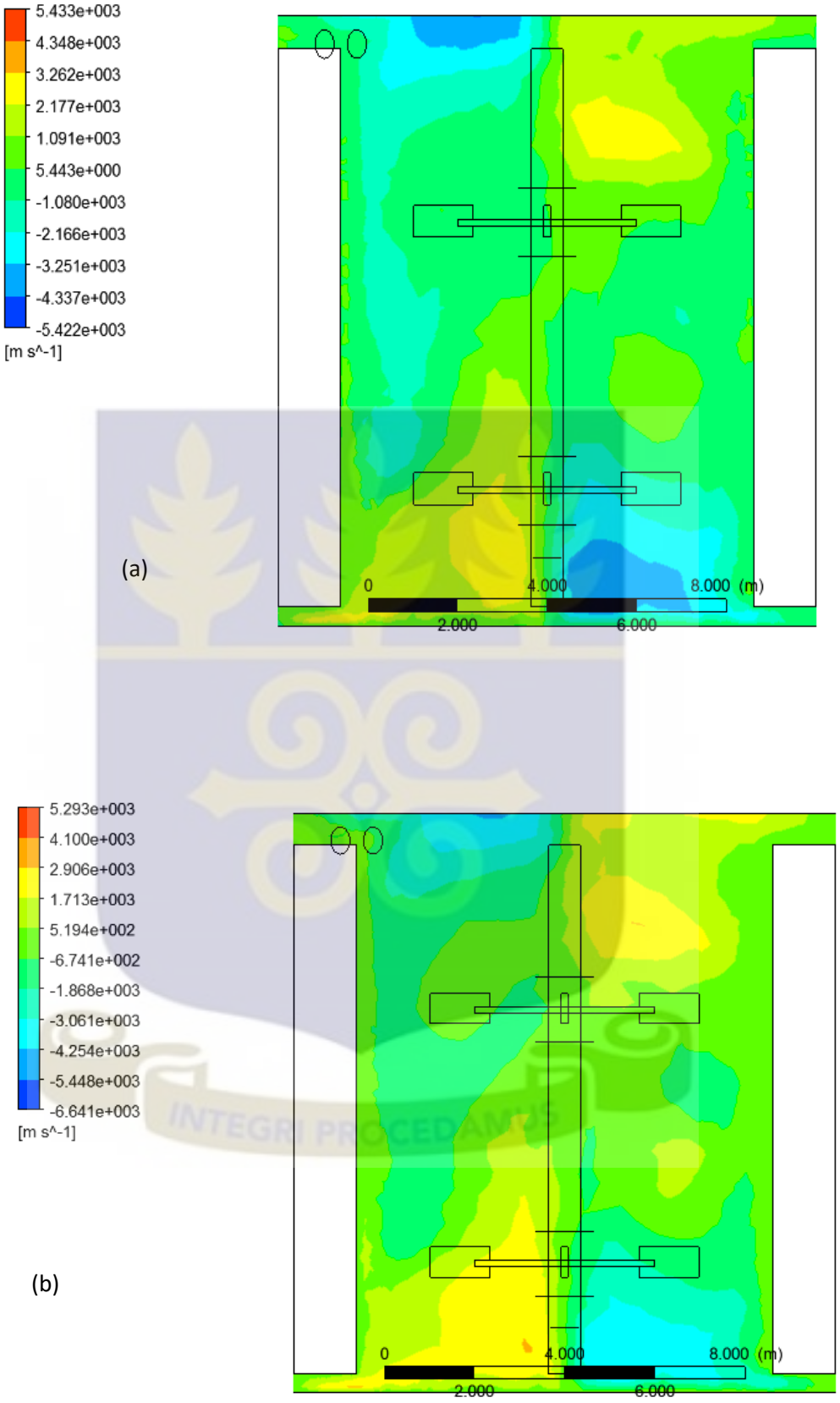

Figure 4.12: Radial velocity for Standard $k-\varepsilon$ model; (a) Sand, (b) Water

In comparison, both colour profiles exhibit a generally uneven sand and water radial velocities in the tank. Also both colour profiles show a relatively high axial velocities in the central portions of the tank and a low axial velocities in areas around the bottom right of the tank around the lower section of the shaft.

The RNG $k-\varepsilon$ model of the sand and water radial velocities exhibits a much more uniform radial velocity in the tank domain than the sand and water radial velocities using the standard and the realizable models. A velocity for both sand and water is required for effective mixing to take place.

4.1.2.4 Sand and Water Volume Fraction

Fig. 4.13a represents the vertical contour plot of the x-z plane of sand volume fraction of the realizable $k-\varepsilon$ model with enhanced wall function. The plot shows the extent of sand volume fraction in the leaching tank. It is observed that the sand concentration in the leaching tank is not evenly distributed with relatively a high concentration of sand in the region between the two impellers. The sand volume fraction is also relatively higher at the top of the tank and low at the central portion of the tank. The accumulated sand at the bottom of the tank exhibits that the off-bottom suspension is slightly poor making a portion of the sand settle during mixing.

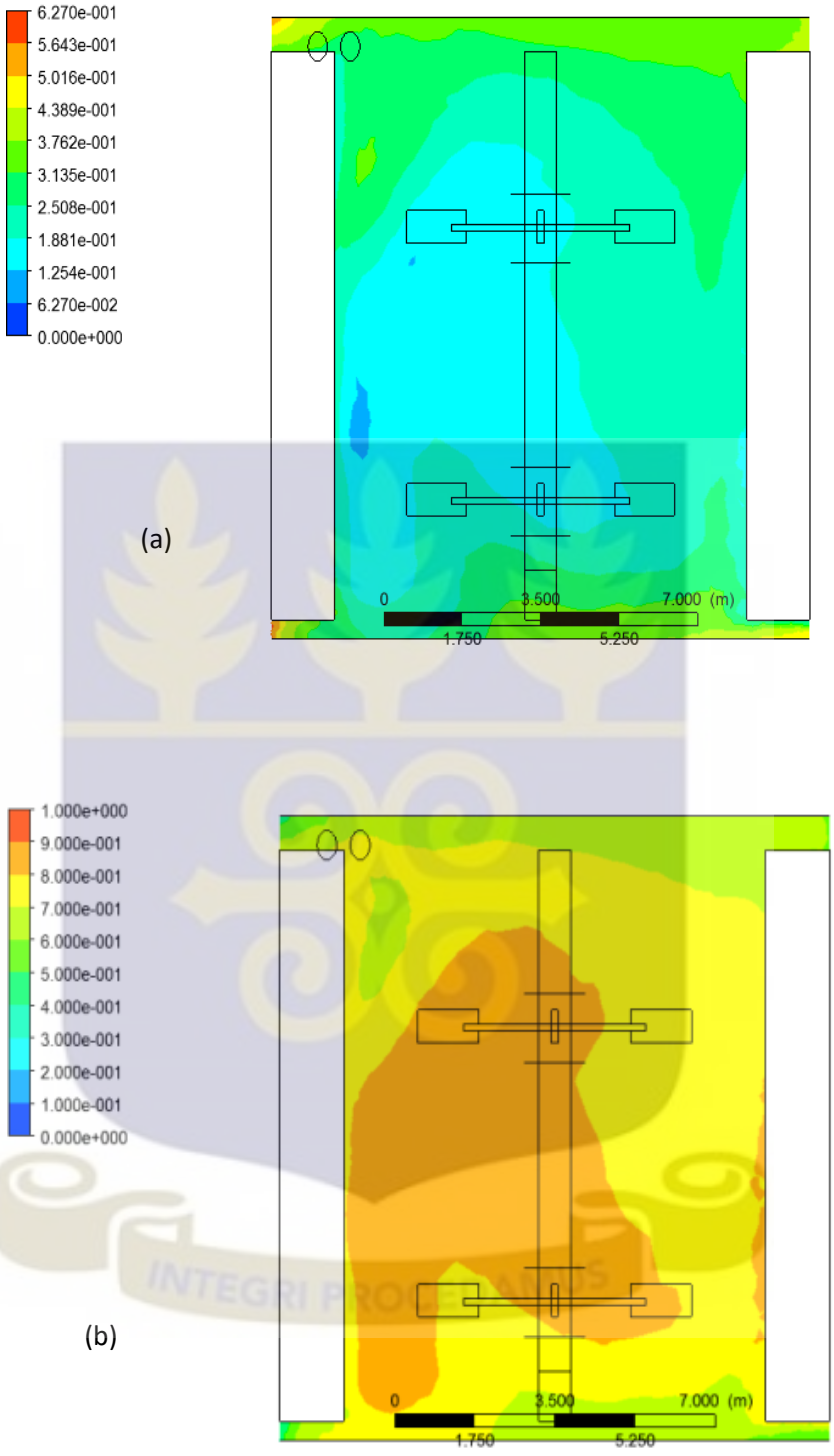

Figure 4.13: Volume fraction for Realizable $k-\varepsilon$ model; (a) Sand, (b) Water

Also in Figure 4.13b, it can be observed that the water concentration inside the tank is generally high but with little variations. The central portion of the tank around the impeller shaft and near the left side of the baffle is high indicating more water volume fraction than sand. The bottom and the topmost part of the tank indicates low concentration of water in those regions which is an indication of sand concentration at the bottom of the tank which can cause settling of the sand.

It can be observed that the water volume is higher than the sand volume fraction especially in areas around the center left of the tank using the realizable $k-\varepsilon$ model.

Figure 4.14a also represents the vertical contour plot of the x-z plane of sand volume fraction of the RNG $k-\varepsilon$ model with enhanced wall function. From the contour plot in Figure 4.14a, there is a slightly high concentration of sand at the bottom and at the topmost left of the tank. The colour intensity at the bottom and the topmost left of the tank are higher compared the central portion of the leaching tank. This means that there is no off-bottom suspension and the mixing is not uniform in the tank.

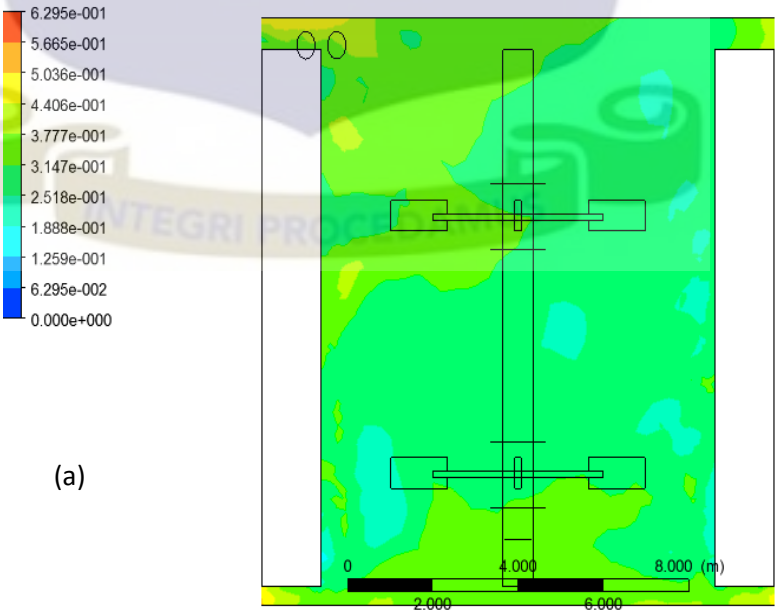

(a)

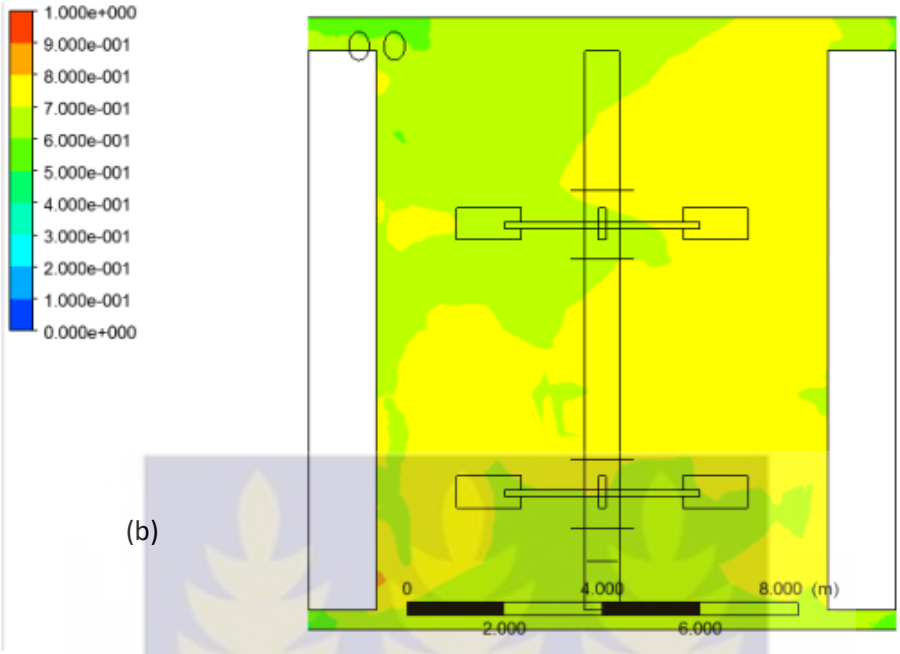

Figure 4.14: Volume fraction for RNG $k-\varepsilon$ model; (a) Sand, (b) Water

Similarly, Figure 4.14b signifies the inhomogeneous mixing of the water volume fraction in the tank domain. The water volume fraction around the central point near the bottom and the topmost left corner of tank have low water volume fraction. The central portion toward the top right corner of the tank represents high water volume fraction. The difference in the water volume fraction in the tank is seen by the two different colour profile of the leaching tank.

However comparing the volume fraction profiles of sand and water in Figures 4.14a and 14.b respectively, it can be seen that the water volume fraction in the tank is higher than the sand volume fraction in the same tank particularly around the central portion of the leaching tank using the RNG $k-\varepsilon$ model.

Figure 4.15a also represents the vertical contour plot of the x-z plane of sand volume fraction of the standard $k-\varepsilon$ model with enhanced wall function. This represents a

slightly uniform mixing with a slightly good off-bottom suspension. This is evident from the Figure in the generally uniform colour intensity in the colour contour.

There is also a high material concentration at the top of the tank indicating uneven distribution of ore slurry in the tank. This high material concentration at the top of the tank is indicated in the colour contour by the high colour intensity in the Figure above.

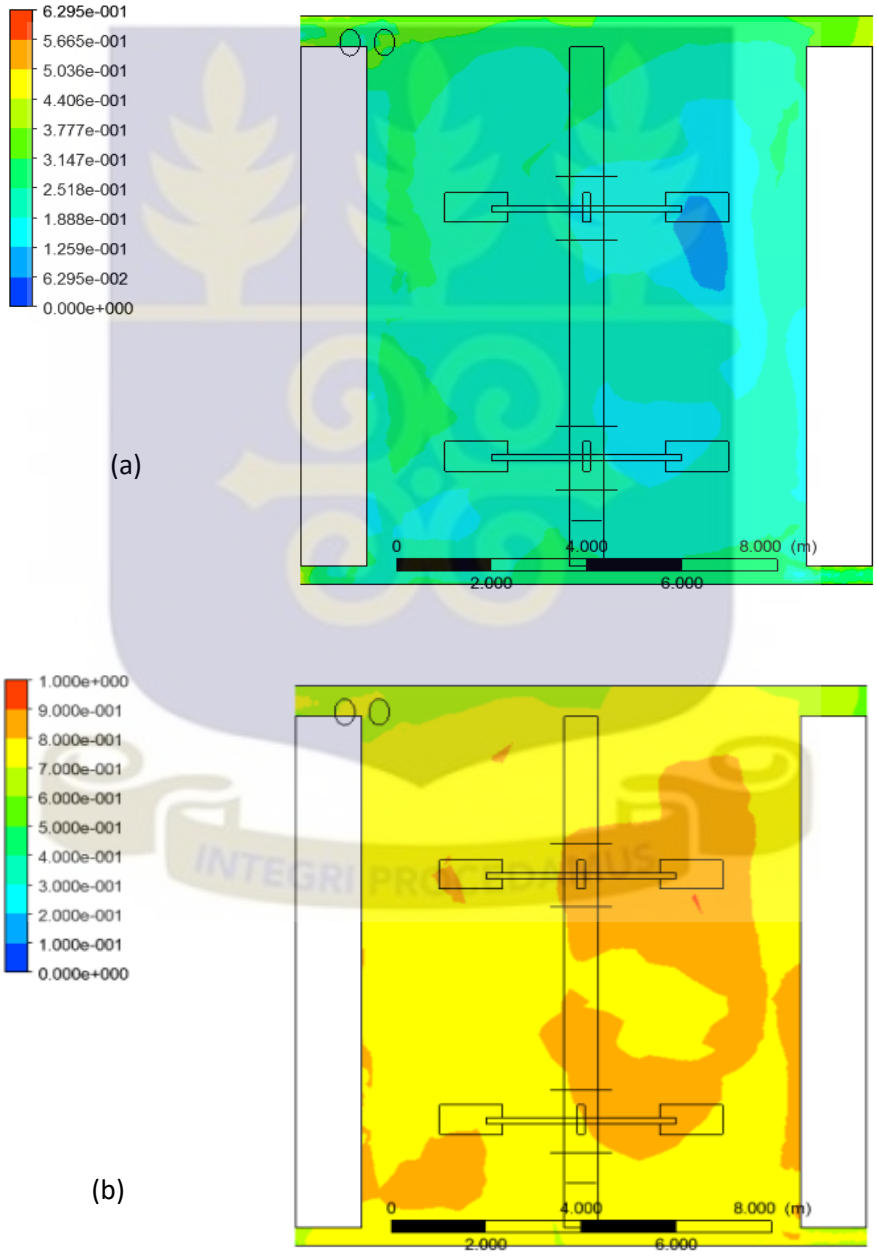

Figure 4.15:Volume fraction for Standard $k-\varepsilon$ model; (a) Sand, (b) Water

Figure 4.15b represent the water volume fraction using the same standard $k-\varepsilon$ model. The colour profile indicates generally a high water volume fraction in the tank with the exception of the right portion of the tank around the impeller region which has a very high water volume fraction. The difference in the water volume fraction is evident in the colour difference between the right portion of the impellers and the entire tank of the colour profile in the diagram.

Relating the two Figures in 4.15, it can be deduced from the colour contours that there is a higher water volume fraction in the tank than the sand volume fraction in the same tank using the standard $k-\varepsilon$ model.

In terms of the volume fractions of the sand and water in the tank domain, the RNG model gives a better colour profile indicating a better sand/water mixing. This is because the colour profile of the RNG $k-\varepsilon$ model indicates a small differential in volume fraction of both sand and water at any point in the tank domain than the two other models.

4.1.2.5 Eddy Viscosity of Water

Figures 4.16a and 4.16c represents the contour plot of eddy viscosity of the material in the leaching tank using realizable $k-\varepsilon$ and standard models. From the diagrams, the eddy viscosity of the material is uniformly high in the domain of the tank except some small portion at the base of the shaft and top of the tank in Figure 4.16a. The even distribution of the eddy viscosity on the colour contour is visible in the uniform colour in the profile below.

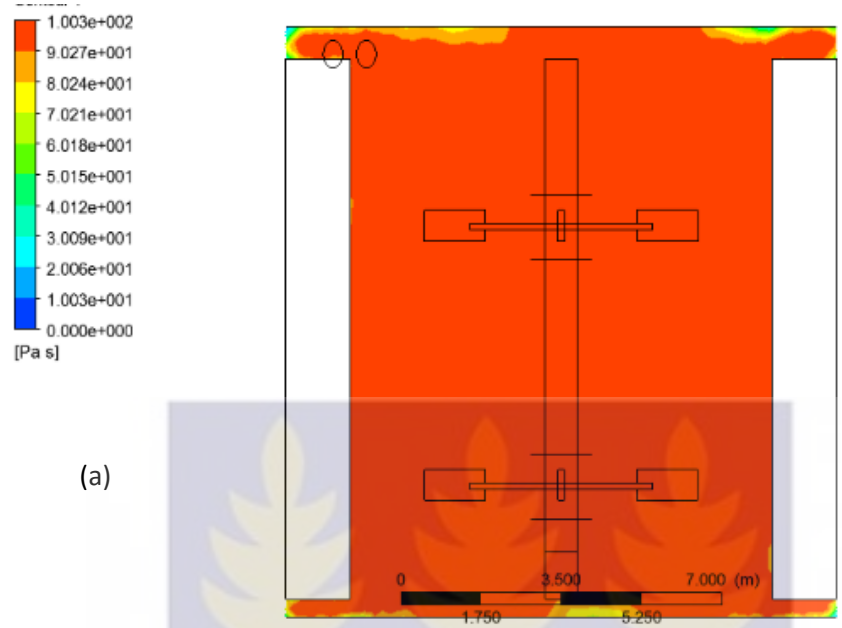

(a)

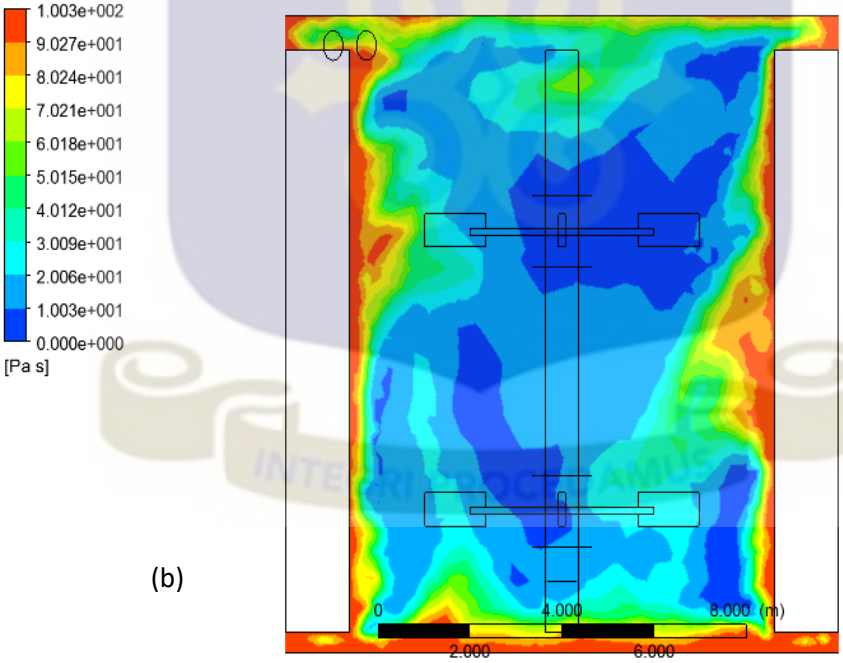

(b)

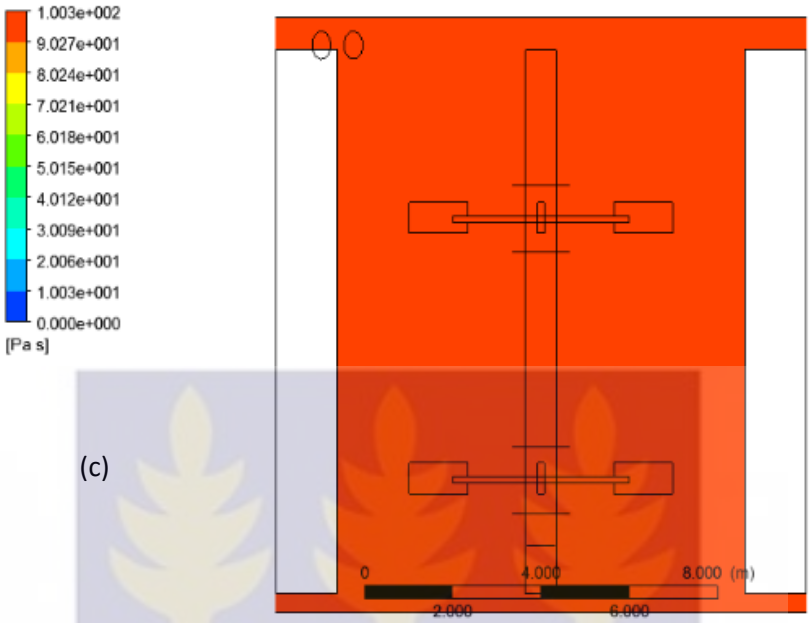

Figure 4.16: Eddy viscosity; (a) Realizable $k-\varepsilon$ model, (b) RNG $k-\varepsilon$ model, (c) Standard $k-\varepsilon$ model

Contrary to the observation in Figures 4.16a and 4.16c, Figure 4.16b depicts the eddy viscosity profile using RNG $k-\varepsilon$ model of the material in the tank. It can be observed the eddy viscosity is high along the walls and the top of the tank. The central portion of the tank generally showed low eddy viscosity especially areas around the upper part of the shaft towards the right impeller and areas near the bottom left of the tank. This uneven distribution of eddy viscosity is seen in the contour profile by the different patches of colours in Figure 4.16b contrary to the uniformly high eddy viscosity in Figures 4.16a and 4.16c.

Since eddy viscosity is synonymous to turbulence, a high eddy viscosity impacts positively on the mixing process. In the colour profiles discussed in Figures 4.16, it can be seen that the realizable and the standard models shows high eddy viscosities.

4.2.1.6 Turbulent Kinetic Energy

The Figures 4.17a, 4.17b and 4.17c represents the realizable model, RNG $k-\varepsilon$ model and standard $k-\varepsilon$ model respectively of the turbulent kinetic energy of the leaching tank. The colour contours above show that the turbulent kinetic energy is zero.

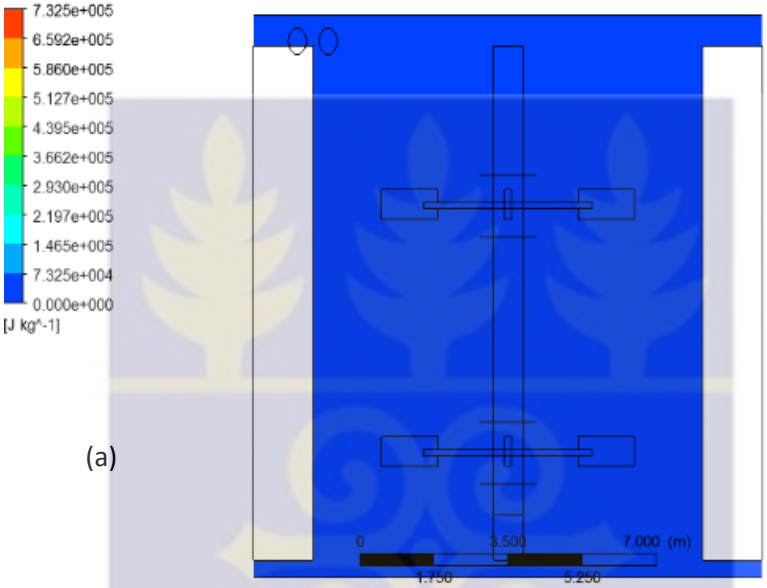

(a)

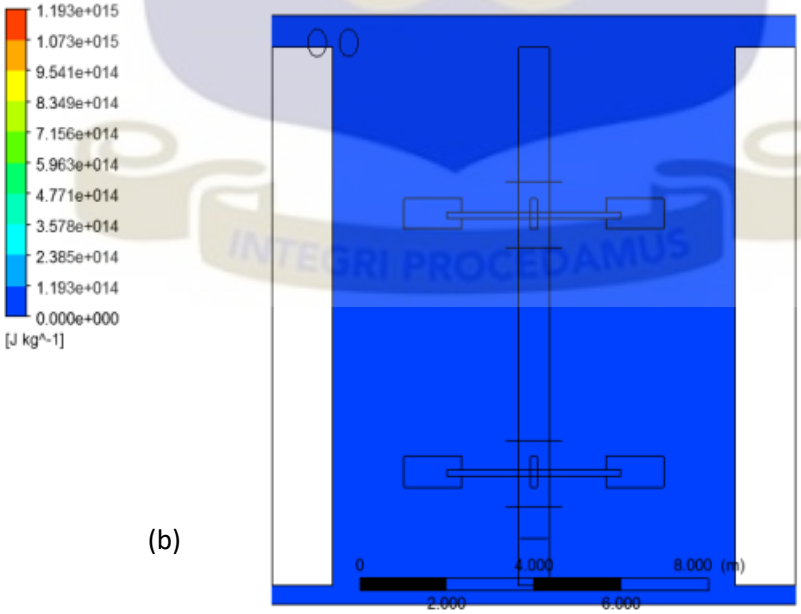

(b)

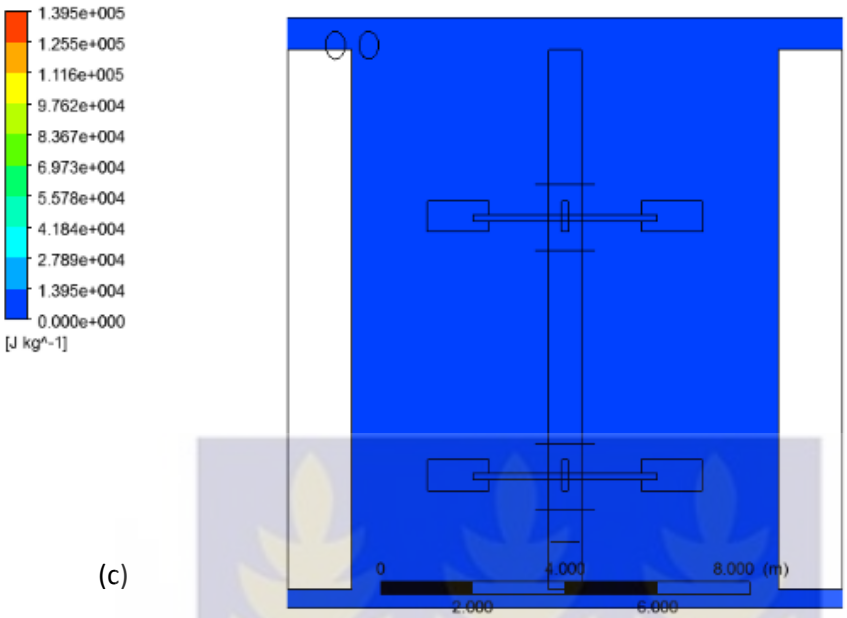

(c)

Figure 4.17: Turbulent kinetic energy; (a) Realizable model, (b) RNG model, (c) Standard model

CHAPTER FIVE

CONCLUSIONS AND RECOMMENDATIONS

This Chapter presents the outcome of the present study, recommendations as well as suggestions for future study

5.1 CONCLUSIONS

Computational Fluid Dynamics codes have been used to simulate the flow pattern of a mixing process typically experienced in a gold leaching (stirred) tank using an Eulerian-Eulerian multi-fluid model to extend mixing behaviour. The simulations have been performed with various RANS models to understand the effects of such models on mixing. Standard k-ε, Realizable $k-\varepsilon$ model and RNG $k-\varepsilon$ model have been simulated and tested in this thesis. The main conclusions drawn from this study are as follows:

1. Circulation loops within the flow field resulted in flow segregation within the tank
2. Velocity contour plots reveal minimum deposition of sand particles on the bottom of the tank. This is due to the strong tangential velocity component, of the impeller discharge.
3. The standard $k-\varepsilon$ model and the realizable $k-\varepsilon$ model predicted higher velocities than the RNG $k-\varepsilon$ model. With the RNG $k-\varepsilon$ model, the eddy viscosity is higher around the tank walls of the vessel.
4. From the eddy viscosity profiles, the standard and the realizable $k-\varepsilon$ predicted a better degree of mixing.

In general, the CFD approach gave a better description of the flow structure in a leaching tank and could therefore be used for industrial flow analysis instead of experimental methods that are not only cost intensive but also do not provide any clear picture of the flow field. The CFD approach is necessary for effective design of flow systems and validation of design data especially after process intensification.

5.2 RECOMMENDATIONS

After successfully simulating mixing and understanding fluid flow patterns in the stirred tank, the following suggestions are needed to be carried out in the future.

1. The mixing behaviour of CSTR should be studied both experimentally and numerically.
2. The modelling and simulation study of flows with different impeller configuration to understand the effect of impeller on mixing.

REFERENCES

Alcamo, R., Micale, G., Grisafi, F., Brucato, A. and Ciofato, M. (2005). Large Eddy Simulation of Turbulent Flow in an Unbaffled Stirred Tank Driven by a Rushton Turbine. Chemical Engineering Science, 60, 2303-2316.

Anderson, K., and Londerville, S. (2013). Practical Use of Computational Fluid Dynamics to Industrial Combustion Applications. American Flame Research Committee Combustion Symposium, (September).

Angst, R., Harnack, E., Singh, M. and Xuereb, C. (2001). Eulerian Simulation of Dense Solid-liquid Suspension in Multi-Stage Stirred Reactors Proceedings of 11th European Conference of Mixing, Bambarg, 14-17.

ANSYS CFX Introduction, 2012.

Ansys Fluent (2012). User Guide (Release 15.0), Multiphase Flows. ANSYS Inc., (April), Chapter 17.

Aubin J., Fletcher D. F. and Xuereb C (2004). Modeling Turbulent Flow in Stirred Tanks with CFD : The Influence of the Modelling Approach, Turbulence Model and Numerical Scheme. 445, 431–445.

Batchelor, G.K., An introduction to Fluid Dynamics. Cambridge Univ. Press, Cambridge, England, 1967.

Bhatt, B., and Agrawal, S. S. (1980). Pharmaceutical engineering. Bollettino Chimico Farmaceutico, 119(10), 8.

Brucato, A., Ciofalo M., Grisafi, F. and Micale G. (1994). Complete numerical Simulation of Flow in baffled Stirred Vessel: inner-outer approach. Inst. Chem. Eng. Symp. 136, 155-162.

Castro, N. F., Chitra, B., Pushpalatha, R., and Sudalai, S. (2015). Heat transfer Effects for two different impellers using Newtonian and Non-Newtonian fluids in an Agitated Vessel, 7(6), 2802–2808.

Cheremisinoff, N. P. (2000). Mixing Equipment. Handbook of Chemical Processing Equipment. http://doi.org/http://dx.doi.org/10.1016/B978-075067126-2.50008-6

Coker, A. K. (2001). Modeling, Simulation, and Operation of a Sabatier Reactor. Industrial & Engineering Chemistry Process Design and Development (Vol. 13). http://doi.org/10.1021/i260051a007

Devi, T., and Kumar, B. (2012a). CFD simulation of flow patterns in unbaffled stirred tank with CD-6 impeller. Chemical Industry and Chemical Engineering Quarterly, 18(4-1), 535–546. http://doi.org/10.2298/CICEQ111130029D

Devi, T., and Kumar, B. (2012b). CFD simulation of flow patterns in unbaffled stirred tank with CD-6 impeller. Chemical Industry and Chemical Engineering Quarterly, 18(4-1), 535–546. http://doi.org/10.2298/CICEQ111130029D

Dong, L., Johansen, S.T. and Engh, T.A., 1994, "Flow induced by an Impeller in an unbaffled tank-2. Numerical Modelling," Chemical Engineering Science, Vol. 49, pp. 3511-3518.

Ferreira, L. S., and Trierweiler, J. O. (2009). Modeling and simulation of the polymeric nanocapsule formation process. IFAC Proceedings Volumes (IFAC-PapersOnline), 7(PART 1), 405–410. http://doi.org/10.1002/aic

FLUENT, A. (2009). User's Guide, (April).

G. Montante, K. Lee, C. A. Brucato, M. Yianneskis, Can. J. Chemical Eng. 77. (1999) 649-659.

Gurmen, F. &. (2008). ChE 344 - Mixing in Chemical Reactors. Michigan.

Hiltunen, K., Kallio, S., Karema, H., Kataja, M., Koponen, A., Manninen, M., and Taivassalo, V. (2009). Multiphase Flow Dynamics Theory and Numerics.

Holloway, M. D., Nwaoha, C., and Onyewuenyi, O. A. (n.d.). Process Plant Equipment.

Javed, K.H., Mahmud T. and Zhu J.M., (2006). Numerical Simulation of Turbulent Batch Mixing in a Vessel agitated by Rushton Turbine, Chem. Eng. Process. 45 (2), 99-112.

Kars-jordan, F., and Hiltunen, P. (2007). Agitation Handbook Filipp Kars-Jordan Petri Hiltunen.

Khorkpor, A. R., 1, P.Mavros, 2, Ranade, V. V., 1, and BERTRAND, *and J. (2004). Simulation of Flow Generated by An Axial-Flow Impeller Batch and Continuous Operation. Chemical Engineering, 82(June), 737–751. http://doi.org/10.1205/026387604774196028

Kuncewicz, C.Z. 1997 "Modelling of liquid Flow in a Mixer in the laminar flow," PhD Thesis, pp. 766.

Launders and D.B. (1972). Spalding. Lectures in Mathematical Models of Turbulence Academic Press, London, England.

Lee, K.C., Ng, K. and Yianneskis, M., 1996, "Sliding mesh predictions of the flows around Rushton Impellers," IChemE. Symposium Series, Vol 140, pp. 1-12.

Lopez de Bertodano, M. (1992) Turbulent Bubbly Two-phase Flow in a Triangular Duct. PhD Dissertation, Rensselaer Polytechnic Institute, Troy, New York.

Middleton, J.C., Peirce, F. and Lynch, P.M., 1986, "Computation of flow fields and complex reaction yield in turbulent stirred reactors and comparison with experimental data," Chemical Engineering Research Design, vol 64, pp.18-22

Mohd Rizal Mamat @ Ibrahim, Azraf Azman, N. O. (2013). Residence Time Distribution (RTD) Prediction in Mixing Vessel via CFD Simulation Using Fluent :

Molnár, B., Egedy, A., and Varga, T. (2013). CFD model based comparison of mixing efficiency of different impeller geometries. Chemical Engineering Transactions, 32, 1453–1458. http://doi.org/10.33032/CET1332243

Muzzio, F. J., Alexander, A., Goodridge, C., Shen, E., and Shinbrot, T. (2004). Solids Mixing. Handbook of Industrial Mixing. Science and Practice. http://doi.org/10.1002/0471451452

Myers, K. J., Reeder, M. F., and Fasano, J. B. (2002). Optimize mixing by using the proper baffles. Chemical Engineering Progress, 98(2), 42–47.

Oden, J. T., and Prudhomme, S. (2002). Mathematical Perspectives on Large Eddy, 1–45.

Pordal, H. S., and Matice, C. J. (2003). Multi-tiered Solution Technique for Design, Analysis and Scale-up of Mixing Processes. Chemical Processing Magazine, 1–9.

Prasanna, G., Prasad, G., Pravin, R., Sanket, M., and Deshpande, P. (2016). Design and Manufacturing of Chemical Agitator, (3), 3093–3098.

Rabiner, L. R., and Gold, B. (1985). t i , i : I, 6(0), 1308–1310.

Rajavathsavai, D., Khapre, A. and Munshi, B., 2013, "Study of Mixing Behaviour of a CSTR using CFD". Department of Chemical Engineering, National Institute of Technology, Rourkela, 769008, Orissa, India.

Rigby, G.D., Evans, G.M. and Jameson, G.J., 1997, "Bubble breakup from ventilated cavities in Multiphase Reactor, Chemical Engineering Science, Vol. 52, pp. 3677-3684.

Stenmark, E. (2013). On Multiphase Flow Models in ANSYS CFD Software.

Stenmark, Elin (2013) on Multiphase Flow Models in ANSYS CFD Software Department of Applied Mechanics Division of Fluid Dynamics Chalmers University of Technology Goteburg, Sweden.

Tabor, A., Gosman, A.D. and Issa, R.A., 1998, Numerical Simulation of the Flow in a Mixing Vessel Stirred by a Rushton Turbine," IChemE Symposium series, Vol. 140, pp. 25-34.

Udaya B. R., Gopalakrishnan S, Ramasamy E., 2003, "Computational Fluid Dynamic Analysis of Turbulence Effect on Reaction in Stirred Tank Reactors", Department of Chemical Engineering, Coimbatore Institute of Technology, Coimbatore-641014, India.

Huang W, and Li, K. "CFD Simulation of Flows in Stirred Tank Reactors Through Prediction of Momentum Source Department of Geochemistry and Environmental Science, University of Science and Technology of China, P.R. China (2013).

Xiao-chang, C., Ting-an, Z. and Qiu-yue, Z., Computational Simulation of fluid dynamics in a tubular stirred reactor. Transactions of Nonferrous Metals Society of China, 19, 489-495 (2009).

Yoon, H.S., Sharp, K.V., Hill, D.F., Adrian, R.J., Balachander, S., Ha, M.Y. and Kar, K. (2001). Integrated and Experimental Computational Approach to Simulation of Flow in a Stirred Tank. Chemical Engineering Science, 56, 6635-6649.

Yusof, A. A., Wasbari, F., Saadun, M. N. A., and Zakaria, M. S. (2014). Part 1 FLUID POWER SYSTEM Introduction to Fluid Power System.

APPENDIX

DEFINITION OF TERMS

Processing Time it is the interval during which a material is changed from one form to another that is more inputs are transformed into a finish product by a manufacturing procedure.

Process Operation also called process manufacturing or process production method is the mass production method of producing products in a continuous flow.

Phase or state of matter is a domain within a many-body system within which relevant physical properties are uniform. Relevant properties may include chemical composition, density and stoichiometry.

Homogeneous Fluid is a fluid in one phase.

Mass Transfer describes the transport of substance from one point to another either in single phase or multiphase.

Mixing Tank/Vessel/Reactor is a machine container that is used to blend various components together.

Ore is a naturally occurring mineral rock which a metal or valuable mineral can be extracted from.

Adsorption Tank is a container in which there is adhesion of gold particles onto activated charcoal.

Slurry is a semi-liquid mixture typically of sand and water.

Troubleshooting is the process of analysing, detecting and solving problems involving a process of elimination.

Steady State is a condition of a system or process that does not change in time. Example temperature, pressure etc.

Incompressible Fluid is a fluid with a constant density whose volume does not change with pressure. Incompressible fluids do not exist; this behaviour, however, may be assumed in some cases to simplify the derivation and the final form of many flow equations.

Compressible Fluids: these are fluids that experience large change in volume as a function of pressure, water etc.

Simulation is the use of computer to calculate by means of extrapolation the effect of a given physical process.

Agitation is the process of stirring things up to obtain a uniform mixture.

Leaching is the extraction or dissolution of certain materials from a carrier into a liquid.